Band Structure and Fermi Surface of Ferromagnetic Nickel*

E. I. ZORNBERG†‡
The James Franck Institute and Department of Physics, The University of Chicago, Chicago, Illinois 60637
(Received 24 March 1969; revised manuscript received 3 June 1969)

The band structure and Fermi surface of ferromagnetic Ni were studied using Mueller's combined interpolation scheme, extended to include spin-orbit and exchange interactions. Uniform exchange splittings were included in the molecular-field approximation. Semiempirical band structures were obtained which gave *detailed* agreement with experimental data where they were available, and *over-all* agreement with the results of *ab initio* calculations. In particular, good fits were obtained to the X pocket and L-neck de Haas–van Alphen data, magnetic breakdown effects, optical edges, and valence (i.e., 10.00 electrons/atom). It was possible to fit the X pocket Fermi surface using a "partial" two-center approximation to the tight-binding d parameters. The X_5 quasiellipsoidal pocket was found to have an unusual shape, resulting from anisotropic interaction with the neighboring X_2 band. Moreover, the d bands were sufficiently high in energy that the X pocket had some s-p character along its major axis. Many-body mass enhancement factors were found to be nearly uniform (≈ 2) after the light-mass s-p character was added to the X pocket. For the d-band exchange splittings, values of 0.4–0.6 eV were found, depending on assignments of optical edges. The density of states showed a sharp multipeaked structure, which, when smeared out, gave qualitative agreement with the density of states obtained from recent ultraviolet photoemission studies.

I. INTRODUCTION

THE electronic structures of noble and near-noble transition metals have been the subject of extensive study.[1–8] With the computational success of the augmented-plane-wave (APW)[9] and Korringa-Konn-Rostoker (KKR)[10,11] methods, energy bands derived from plausible one-electron potentials have become available for a number of such metals.[1–8] Refinements in experimental techniques have produced a growing body of data (especially extremal cross-sectional areas) on the Fermi surfaces of these metals.[12–21] The picture that emerges from comparing the theoretical band structures with the experimental data is one of general qualitative success of the itinerant one-electron model.[1,22]

The object of this paper is to explore this comparison quantitatively for a ferromagnetic material. An attempt is made to construct a *complete* ferromagnetic band structure for Ni which gives agreement with available data, in particular Fermi-surface,[14–19] optical,[23,24] and saturation magnetization data.[25,26] Such a band structure is wanted to fit the data [especially de Haas–van Alphen (dHvA) data] where it is available and to agree qualitatively with the results of *ab initio* calculations throughout the Brillouin zone.

Ab initio calculations on Ni have been made by Hanus,[4] who studied paramagnetic Ni, and by both Wakoh[6] and Connolly,[8] who did self-consistent calculations on ferromagnetic Ni. Hodges, Ehrenreich, and Lang[27] (HEL) used an interpolation scheme approach (see below) to obtain ferromagnetic Ni bands. All of these calculations gave qualitative agreement with early experimental data[17–19]; however, they all ignored the small but important effects arising from the *com-*

* Submitted in partial fulfillment of the requirements for the degree of Doctor of Philosophy at the University of Chicago.
† General Electric Fellow 1965–66.
‡ Present address: Dept. of Physics, Wellesley College, Wellesley, Mass.

[1] For a general review of the electronic structure of transition and noble metals, see M. H. Cohen and F. M. Mueller, *The Atomic and Electronic Structure of Metals* (The American Society for Metals, Cleveland, Ohio, 1967).
[2] G. A. Burdick, Phys. Rev. **129**, 138 (1963).
[3] B. Segall, Phys. Rev. **125**, 109 (1962).
[4] J. G. Hanus, MIT Solid State and Molecular Theory Group Quarterly Progress Report, 1962 (unpublished).
[5] S. Wakoh and J. Yamashita, J. Phys. Soc. Japan **19**, 1342 (1964).
[6] S. Wakoh, J. Phys. Soc. Japan **20**, 1894 (1965).
[7] E. C. Snow, J. T. Waber, and A. C. Switendick, J. Appl. Phys. **37**, 1342 (1966).
[8] J. W. D. Connolly, Phys. Rev. **159**, 415 (1967). We thank Dr. Connolly for a preprint of this work and a list of his eigenvalues.
[9] J. C. Slater, Phys. Rev. **51**, 846 (1937); **92**, 603 (1953).
[10] J. Korringa, Physica **13**, 392 (1947); with Ref. 11, referred to as KKR.
[11] W. Kohn and N. Rostoker, Phys. Rev. **94**, 1411 (1954).
[12] For a review of experimental methods, see D. Shoenberg, in *Proceedings of the Ninth International Conference on Low Temperature Physics*, edited by J. G. Daunt (Plenum Press, Inc., New York, 1965), p. 665; E. Fawcett, Advan. Phys. **13**, 139 (1964); R. W. Stark and L. R. Windmiller, Cryogenics **8**, 272 (1968).
[13] D. Shoenberg, Phil. Trans. Roy. Soc. London **A255**, 85 (1962).
[14] D. C. Tsui, Phys. Rev. **164**, 669 (1967).
[15] D. C. Tsui and R. W. Stark, Phys. Rev. Letters **17**, 831 (1966); R. W. Stark and D. C. Tsui, J. Appl. Phys. **39**, 1056 (1968).
[16] L. Hodges, D. R. Stone, and A. V. Gold, Phys. Rev. Letters **19**, 655 (1967). We thank Dr. Hodges for sending us a preprint of this work and a list of his d-band parameters.
[17] A. S. Joseph and A. C. Thorsen, Phys. Rev. Letters **11**, 554 (1963).
[18] E. Fawcett and W. A. Reed, Phys. Rev. Letters **9**, 336 (1962).
[19] E. Fawcett and W. A. Reed, Phys. Rev. **131**, 2463 (1963).
[20] J. J. Vuillemin, Phys. Rev. **144**, 396 (1966).
[21] L. R. Windmiller and J. B. Ketterson, Phys. Rev. Letters **20**, 324 (1968).
[22] C. Herring, *Magnetism* (Academic Press Inc., New York, 1966), Vol. IV, Chaps. VI and VIII.
[23] H. Ehrenreich, H. R. Philipp, and D. J. Olechna, Phys. Rev. **131**, 2469 (1963).
[24] J. Hanus, J. Feinleib, and W. J. Scouler, Phys. Rev. Letters **19**, 16 (1967).
[25] H. Danan, A. Herr, and A. J. P. Meyer, J. Appl. Phys. **39**, 669 (1968).
[26] G. Fischer, A. Herr, A. J. P. Meyer, J. Appl. Phys. **39**, 545 (1968).
[27] L. Hodges, H. Ehrenreich, and N. D. Lang, Phys. Rev. **152**, 505 (1966).

bined effect of spin-orbit coupling, internal magnetization, and externally applied magnetic fields. Hodges, Stone, and Gold[16] (HSG) included these effects to fit dHvA data in a small region of the Brillouin zone (BZ); however, their over-all band structure was qualitatively different from the results of the *ab initio* calculations. Here band structures are presented which include these effects, which agree in detail with a wide range of data, and which are in over-all agreement with the results of *ab initio* calculations.

The ferromagnetism of Ni destroys time-reversal symmetry and results in the splitting of the up- and down-spin bands.[22] This ferromagnetic or exchange splitting produces a band structure with an excess of electrons of one spin. In turn, the excess of spins can be considered to produce the exchange field which makes the ferromagnetic state energetically favored at low temperatures.

A central goal of the present analysis is the establishment of the ferromagnetic exchange splittings[22,28] of the d levels of Ni near the Fermi energy. To determine this quantity from general theoretical considerations by construction of an accurate one-electron potential is quite difficult. In practice[5,6,8] the nonlocal exchange and correlation operators are usually replaced by an effective local potential $V_{ex}(r)$, chosen to simulate the exchange potential of a free-electron gas having a density equal to the crystalline change density $\rho(r)$.[29,30] When $\rho(r)$ varies rapidly—as it does for the d electrons in a transition metal—the errors incurred in this statistical approximation are difficult to estimate. Indeed for a given crystal there may be no local exchange potential consistent with its observed Fermi surfaces.

In view of these complications it appears desirable to develop an alternative approach which stresses (insofar as possible) an inductive analysis of the available data (particularly the detailed dHvA data) within a general analytic framework.[31] One such procedure would be to vary the potential or phase-shift input to the APW and KKR programs until agreement with Fermi-surface radii or areas is obtained. Recently, this procedure has been worked out for the APW method, and has been applied successfully to Cu and the alkali metals.[32]

Another procedure, in a more advanced stage of development, follows the spirit of the pseudopotential[33,34] approach which has been so successful in explaining the electronic properties of some simple metals and semiconductors. Pseudopotential theory provides a simple and economical way of calculating energy bands anywhere in the BZ in terms of a few parameters. These parameters (pseudopotential form factors) provide a convenient characterization of the material.[34] They also serve to limit arbitrary variation of the band structure and for this reason may be regarded as constituents of a model Hamiltonian[35] for quasiparticles.

In the present work Mueller's combined interpolation scheme[36] is used as a model Hamiltonian. A similar scheme has been developed by HEL.[27] Mueller has shown that the energy bands of Cu can be described quite accurately in terms of 10 to 15 parameters specifying the d bands, s-p conduction bands, and the conduction-band–d-band interaction. Such schemes for transition metals have been analyzed by several workers.[37–39]

It is feasible for simple metals to determine the s-p pseudopotential parameters directly from experiment and thus obtain an empirical band structure.[34] At present this is not possible for Ni because of the large number of parameters and limited available data. Instead we start with parameters obtained from fitting a number of first-principles calculations. The parameters are then varied, subject to *specified constraints*, until agreement with experiment is obtained. These constraints may make it difficult or impossible to fit some of the data. It must then be decided whether to reject either the data (or their interpretation) or the constraints.

In Sec. II, we present the results of an APW calculation for paramagnetic Ni which enable us to compare the parameters in Ni with those in Cu. The paramagnetic nickel parameters serve as a starting point for our calculation.

With Mueller the interpolation scheme has been extended to include spin orbit and exchange effects.[40] The effects of spin-orbit interaction[16,41] are especially important when studying a hole pocket of the Fermi surface centered at X[42] in the BZ. Unusual properties of the dHvA data for the pocket are explained in Sec. III.

It is believed that besides this hole pocket, there exist three large Γ-centered electron surfaces,[5,8,14,27] one of which contains a "neck" similar to that observed in Cu.[13] Our fit to dHvA data[14,17] for this neck is discussed in Sec. VI. Two additional small hole Fermi surfaces near X and L, which are suggested by some calculations,[5,8,27] have not been observed experimentally.[14] The dHvA experiments on the large Fermi surfaces are now in progress.[43]

---

[28] J. C. Slater, Phys. Rev. **49**, 537 (1936).
[29] J. C. Slater, Phys. Rev. **81**, 385 (1951).
[30] W. Kohn and L. J. Sham, Phys. Rev. **140**, A1133 (1965).
[31] E. I. Zornberg and F. M. Mueller, Phys. Rev. **151**, 557 (1966).
[32] M. Lee, Phys. Rev. **178**, 953 (1969).
[33] J. C. Phillips and L. Kleinman, Phys. Rev. **116**, 287 (1959); M. H. Cohen and V. Heine, *ibid.* **122**, 1821 (1961).
[34] For a general review of pseudopotentials, see W. A. Harrison, *Pseudopotentials in the Theory of Metals* (W. A. Benjamin, Inc., New York, 1966).
[35] J. C. Phillips, Advan. Phys. **17**, 79 (1968).
[36] F. M. Mueller, Phys. Rev. **153**, 569 (1967).
[37] V. Heine, Phys. Rev. **153**, 673 (1967).
[38] R. L. Jacobs, Proc. Phys. Soc. (London) **1**, 492 (1968).
[39] J. Hubbard, Proc. Phys. Soc. (London) **92**, 921 (1967).
[40] E. I. Zornberg and F. M. Mueller, Bull. Am. Phys. Soc. **13**, 441 (1968).
[41] R. J. Elliot, Phys. Rev. **96**, 280 (1954); J. Friedel, F. Lenglart, and G. Leman, J. Phys. Chem. Solids **25**, 781 (1964).
[42] Notation from L. P. Bouchaert, R. Smoluchowski, and E. P. Wigner, Phys. Rev. **50**, 58 (1936).
[43] R. W. Stark (private communication).

TABLE I. Parameters of Mueller's combined interpolation scheme obtained from fitting various *ab initio* Cu and Ni band structures. Ni (Z) and Ni(H) were obtained from fitting energies calculated using the APW method in this work and by Hanus, using Hanus's potential (Ref. 4). Ni(Z') was obtained from fitting our energies, giving extra weight to sixth-band energies near 0.60 Ry (see Fig. 1). Cu (l-ind) and Cu (l-dep) were obtained by Mueller, fitting the energy bands of Cu calculated in Refs. 2 and 3. Ni($V_{4\alpha}$) and Ni($V_{4\beta}$) were obtained from fitting the energy bands in Ref. 8.

	Parameter	Units	Ni(Z)	Ni(H)	Cu[a] (l-ind)	Cu[a] (l-dep)	Ni($V_{4\alpha}$)	Ni($V_{4\beta}$)	Ni(Z')
d bands	d_0	Ry	0.532_2	0.501_6	0.438	0.365	0.525_5	0.587_6	0.532_2
	$(dd\sigma)$	Ry	-0.038_1	-0.038_2	-0.025_8	−0.033	−0.033	−0.036	-0.038_1
	$(dd\pi)$	Ry	0.017_3	0.017_4	0.013_2	0.017_6	0.013_2	0.015_5	0.017_3
	$(dd\delta)$	Ry	−0.0017	−0.0019	−0.0015	−0.0029	−0.0009	−0.0017	−0.0017
	γ	Ry	<0.0003	0.0003	0.008	−0.0007	0.0003	0.0003	0.0003
Conduction bands	V_{111}	Ry	0.003	0.042	0.005	0.019	0.033	0.031	−0.006
	V_{200}	Ry	0.026	0.057	0.034	0.040	0.044	0.040	0.015
Orthogonality	A		1.06	1.14	1.29	1.59	0.99	1.30	1.61
	LR_0		3.24	3.11	2.88	3.03	3.00	2.56	2.62
Hybridization	B	Ry	1.31	1.36	1.01	1.02	1.32	1.40	1.475
	LR_1		2.74	2.81	2.93	3.47	2.71	2.69	2.75
β	$\left\lvert\frac{(dd\sigma)}{(dd\pi)}\right\rvert$		2.2	2.2	1.9	1.9	2.5	2.3	2.2

[a] Parameters from Ref. 35.

In Sec. IV, the magnetic breakdown[44] effects observed in the dHvA experiments are discussed.[14–16] The explanation of these effects yields information about the relative positions of the minority spin d band and majority spin conduction band.

Section V deals mainly with the optical data, particularly with two pieces of low-energy structure found in thermoreflectance data.[24] Attempts are made to assign the structure to direct optical transitions. The exchange splittings required to fit the optical assignments are discussed.

In Sec. VI, our band structures which fit the experimental data, are presented, while in Sec. VII, the results of our calculations of effective masses and density of states are presented and compared with experiment.[45]

II. MODEL HAMILTONIAN

We begin this section with a brief description of Mueller's interpolation scheme.[36] The paramagnetic Hamiltonian H_{para} consists of a 9×9 secular determinant. The basis functions are five "tight-binding" d states $\langle d_n|$ and four plane waves (ϕ_{OPW}) which are explicitly orthogonalized to the d states.[46] Instead of using a plane-wave basis set orthogonalized to the s-p core states, small s-p pseudopotential[33,34] parameters V_{111} and V_{200} are used.

[In Sec. IV, it is shown that the addition of two plane waves (making a total of six), degenerate at X, improves the representation of the bands in the magnetic breakdown region near X. Except for the discussion of magnetic breakdown near X, the use of only four plane waves in our Hamiltonian is found to be sufficient.]

The 5×5 d-d block is parametrized in terms of six three-center integrals [so-called Fletcher-Wohlfarth (FW) parameters[47]] or three two-center integrals[48] $(dd\sigma)$, $(dd\pi)$, and $(dd\delta)$. Also included in the d-d block is d_0, the position of the d bands relative to the conduction bands. Mueller also included a small parameter γ to give the correct $\Gamma_{12}-\Gamma_{25'}$ separation. In the process of fitting the APW calculations for Ni (see Table I) this parameter is found to be negligibly small.

In Sec. III, it is shown that making a "partial two-center approximation" using four parameters $(dd\sigma)$, $(dd\pi)$, $(dd\pi')$, and $(dd\delta)$ is convenient for fitting both *ab initio* calculations and experiment. The utility of a strict two-center approximation was discussed by Slater and Koster[48] (SK). In the partial two-center approximation, five of the six FW parameters are obtained from three two-center integrals $(dd\sigma)$, $(dd\pi)$, and $(dd\delta)$, while the sixth (A_4), which would equal $(dd\pi)$ in the strict two-center approximation, becomes an additional parameter. It is called $(dd\pi')$. Both $(dd\pi)$ and $(dd\pi')$ are constrained to be approximately of the same magnitude as derived by fitting energy bands obtained from APW and KKR calculations. Mueller *et al.*[49,50] have found differences between $(dd\pi)$ and $(dd\pi')$ of 10–30%, using the partial two-center approximation in fitting the Pd and Pt band structures.

H_{para} also includes a 4×5 hybridization block. The orthogonality (from the 4×4 block) and hybridization integrals are parametrized in terms of the spherical

[44] For a review of magnetic breakdown, see R. W. Stark and L. M. Falicov, in *Progress in Low Temperature Physics*, edited by C. J. Gorter (North-Holland Publishing Co., Amsterdam, 1967), Vol. V.

[45] D. E. Eastman and W. F. Krolikowski, Phys. Rev. Letters **21**, 623 (1968); D. E. Eastman, J. Appl. Phys. **40**, 1387 (1969).

[46] C. Herring, Phys. Rev. **57**, 1169 (1940).

[47] G. C. Fletcher and E. P. Wohlfarth, Phil. Mag. **42**, 106 (1951); G. C. Fletcher, Proc. Phys. Soc. (London) **A65**, 192 (1952).

[48] J. C. Slater and G. F. Koster, Phys. Rev. **94**, 1498 (1954).

[49] F. M. Mueller, A. J. Freeman, J. O. Dimmock, and A. Furdyna (unpublished).

[50] F. M. Mueller, J. B. Ketterson, L. R. Windmiller, and S. Hornfeldt (unpublished).

Bessel function $j_2(x)$,

$$\langle d_n|\mathbf{k}\rangle \propto AJ_2(kR_0)\,, \tag{2.1}$$

$$\langle d_n|H|\phi_k\rangle \propto BJ_2(kR_1)\,, \tag{2.2}$$

where A, B, R_0, and R_1 are parameters of the interpolation scheme[36] and $\mathbf{k}$ and ϕ_k are the plane wave and OPW of index $\mathbf{k}$, respectively. We have now defined all the parameters in Mueller's 9×9 Hamiltonian for paramagnetic bands.

With Mueller the model Hamiltonian is extended to include both spin-orbit coupling (in the d bands only) and exchange splittings.[40] Mueller *et al.*[49] have verified that the spin-orbit terms involving the s-p conduction bands are small and may be neglected.

The full Hamiltonian can be written[40,51,52]

$$H=H_{\text{para}}+H_{\text{spin-orbit}}+H_{\text{exchange}}\,, \tag{2.3}$$

where

$$H_{\text{para}}=H_{\text{Hartree}}+H_{\text{para exchange}}\,, \tag{2.4}$$

$$H_{\text{spin-orbit}}=\tfrac{1}{2}\zeta\boldsymbol{\sigma}\cdot\mathbf{L}\,, \tag{2.5}$$

$$H_{\text{exchange}}=\frac{[\Delta E-(\boldsymbol{\mu}\cdot\boldsymbol{\beta})]\boldsymbol{\sigma}\cdot\mathbf{H}}{2|\mathbf{H}|} \simeq\frac{\Delta E\boldsymbol{\sigma}\cdot\mathbf{H}}{2|\mathbf{H}|}\,, \tag{2.6}$$

where $\mathbf{B}$ is the magnetic induction, $\mathbf{H}$ is the applied external field, and ΔE is the exchange splitting.

The exchange terms have been treated in a molecular-field approximation, assuming that the effective internal magnetization density lines up with the applied magnetic field. This is justified by the fact that for $\mathbf{H}$ (≃50 kG) parallel to [001], the magnetic field energy density E_H is 100 times greater than the magnetic anisotropy energy density[53–55] E_A. The magnetization density lies along $\mathbf{H}$ if $E_H>6E_A$.

The $\mathbf{k}$-independent exchange splittings for the d- and s-d bands, ΔE_d and ΔE_s are included, in the d and OPW parts of our Hamiltonian, respectively. Thus there are three additional parameters ΔE_d, ΔE_s, and the spin-orbit parameter ζ. With the inclusion of both spins an 18×18 complex secular determinant is solved to find the eigenvalues. The two sets of bands hybridize and most bands will contain electrons of both spins.

If spin-orbit interaction is omitted, in a "rigid-band" approximation, exchange energies can be included *separately* in the ↑ and ↓ bands by shifting the zero of energy and d_0 for each spin. Two 9×9 real secular equations are then solved. This procedure is used in Sec. VI for finding the number of electrons of each spin. Errors of less than 0.01 electrons/atom are incurred in making this approximation.

To obtain a Ni band structure (including energies near the Fermi energy) from which to determine initial values of the interpolation scheme parameters, the APW calculation was redone using Hanus's[4] potential, with the same number of spherical harmonics that Hanus included. The APW programs were supplied to us by Mattheiss and Soven.[56] To test the accuracy of these programs Burdick's[2,57] Cu calculation was repeated, and the results agreed with his within 0.002 Ry.

However, when Hanus's potential was used, our eigenvalues were generally 0.02 Ry lower than his. There were differences of as much as 0.05 Ry between the results of the two calculations for which we have no explanation. Both sets of Ni eigenvalues were used to determine the parameters for Mueller's model Hamiltonian according to the least-squares fitting procedure he describes.[36] The results are shown in Table I, together with parameters for Cu[36] and for Connolly's[8] Ni bands. The strict two-center approximation was used in obtaining the parameters of Table I.

In columns 5 and 6 of Table I the parameters for Connolly's ↑ and ↓ spin bands[8] are compared. From the difference in d_0 for these two spin bands (and zero Γ_1 splitting), it is concluded that Connolly obtained an *average* d-band exchange splitting $\langle\Delta E_d\rangle$ of 0.062 Ry. However, for d bands near the *top* of the d band (e.g., X_5, L_{32}) he obtained an exchange splitting ΔE_d of 0.069 Ry.[8] The difference between ΔE_d and $\langle\Delta E_d\rangle$ is a consequence of the breakdown of the "rigid-band" picture. The majority spin bands (α) are about 10% narrower than the minority spin bands (β). In this work experimental data are considered which give information on bands near E_F, which lies near the top of the d bands. As a result, an estimate of ΔE_d is obtained rather than of $\langle\Delta E_d\rangle$.

Comparing all six calculations in Table I, we find that V_{111} and V_{200}, although shifted from one band structure to the next, always differ by 0.01–0.03 Ry. This indicates that V_{111} and V_{200} fall on an s-p pseudopotential form-factor curve similar to that found for elements (such as Al) not containing d bands near the Fermi energy.[35,58] It suggests that the separation of s-p and s-d interactions into pseudopotential, hybridization, and orthogonality terms proposed by Mueller may be more instructive (and less arbitrary) than the ones proposed by other workers. (They would group the orthogonality terms with the pseudopotential,[27] or the hybridization terms with the pseudopotential terms,[37]

[51] L. M. Falicov and J. Ruvalds, Phys. Rev. **172**, 498 (1968).
[52] J. Ruvalds and L. M. Falicov, Phys. Rev. **172**, 508 (1968).
[53] G. C. Fletcher, Proc. Phys. Soc. (London) **67**, 505 (1954).
[54] R. R. Birss and P. M. Wallis, in *Proceedings of the International Conference on Magnetism, Nottingham, 1964* (The Institute of Physics and the Physical Society, London, 1965).
[55] J. J. M. Franse and G. DeVries, Physica **39**, 477 (1968).

[56] We thank Dr. L. F. Mattheiss and Professor P. Soven for providing us with these programs. We especially thank Professor P. Soven for instruction in their use.
[57] M. I. Chodorow, Ph.D. thesis, MIT, 1939 (unpublished); Phys. Rev. **55**, 675 (1939).
[58] P. J. Lin and J. C. Phillips, Advan. Phys. **14**, 257 (1965).

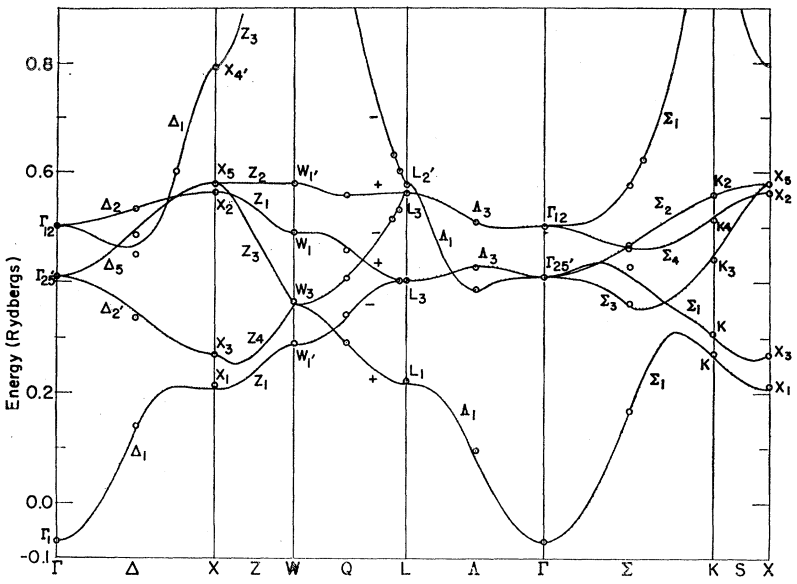

FIG. 1. Combined interpolation scheme fit Ni(Z') to the results of APW calculation (open circles) which used Hanus's potential. Extra weight was given to levels in the sixth band near E_F. The labeling of symmetry points and lines follows Ref. 42.

thereby obscuring the form-factor regularity exhibited in Table I.)

Heine has proposed[37] that, in contrast to the over-all width W of the d band, the ratios of the d band shape parameters $(dd\sigma)$, $(dd\pi)$, and $(dd\delta)$ should be determined primarily by the crystal structure, and should be only a slowly varying function of d_0. This conjecture is largely borne out by the results listed in Table I, although the ratio $\beta=|(dd\sigma)/(dd\pi)|$ is about 20% larger for Ni than for Cu.

The complexity of the s-d hybridization and orthogonality interactions is such that no useful trends have been found for the parameters involved in these terms. The reason for this is that the values change somewhat, depending on whether one chooses to fit levels in the seventh band (second conduction band) which are important, e.g., for the calculation of optical spectra,[59] or levels in the first conduction band only, which are important for the Fermi surface. Thus, in Table I given in column 1 are the parameters for our calculation of Ni, fitting to the first six bands with equal weight, and in column 7 the same bands fitted with the sixth band levels near the Fermi energy given ten times greater weight. The latter fit Ni(Z') to our paramagnetic band structure is shown in Fig. 1. The open circles are the result of the APW calculation. This fit is not as good as Ni(Z) in the hybridization regions of the lower bands, but the sixth band fit has been improved. The rms errors of our fits were $\simeq$0.008 Ry.

As the parameters obtained from fitting our APW calculated bands are varied in order to fit experimental data, the variation is constrained so that the final band structure will be similar to those calculated by solving the Schrödinger equation for reasonable one-electron potentials:

(1) V_{200} is maintained greater than V_{111} by a few hundredths of a Ry.

(2) In view of the success of Heine's conjecture we avoid changing β by more than 20%. Hence a width parameter W is introduced which is initially set equal to 1.00. This parameter multiplies all of the two-center parameters. Then when W is varied, $(dd\sigma)$, $(dd\pi)$, $(dd\pi')$, and $(dd\delta)$ are being varied while keeping their ratios fixed. This parameter W is constrained so that the d bandwidth lies within the range of those calculated for transition metals, i.e., $(0.70<W<1.5)$, depending on the position of the d bands relative to the conduction bands (see Sec. VI).

(3) Implicit in the use of the two-center parameters is the constraint that three-center integrals be small. Equivalently, had the six SK[48] or FW[47] parameters been used, variations in these parameters would be restricted so that the two-center approximation is obeyed. The "partial two-center approximation" is discussed above and in Sec. III.

(4) The $(dd\sigma)$ and $(dd\delta)$ parameters are restricted to be negative, while $(dd\pi)$ and $(dd\pi')$ must be positive.

(5) Generally our parameter changes are constrained to be "small", i.e., to lie within the range of those found from fitting a number of APW calculated band structures.

(6) It is learned from the calculations of Connolly[8] and Wakoh[6] that the s-p exchange splitting ΔE_s is considerably smaller than ΔE_d, $\Delta E_s \lesssim 0.2\Delta E_d$. This corresponds to the s-d exchange being smaller than the d-d exchange. Hence an attempt is made to maintain the condition, $\Delta E_s \ll \Delta E_d$.

III. MINORITY SPIN X POCKET

The analysis of the dHvA data[14] for the X pocket Fermi surface has been given in a preliminary

[59] F. M. Mueller and J. C. Phillips, Phys. Rev. **157**, 600 (1967).

paper.[60] In this section our parameters are presented and the complicated geometry of the X pocket is discussed in detail. Also included is a discussion of the "partial" two-center approximation which was employed in the calculation.

Tsui and Stark[14,15] (TS) and HSG[16] measured extremal cross-sectional areas of light mass quasiellipsoidal hole pockets in two principal symmetry planes. TS concluded that the pockets were centered at X, and were associated with the minority spin light mass band derived from X_5. Hodges *et al.*[16] constructed a local band model (valid only near X) using the HEL[27] interpolation scheme, which explains well certain features of the data. However, apparently in order to explain anisotropies of the ellipsoidal pocket in the plane normal to the principal axis ΓX, they chose tight-binding parameters which do not obey either the strict or partial two-center approximations. As a result they obtain an over-all band structure quite different[60]

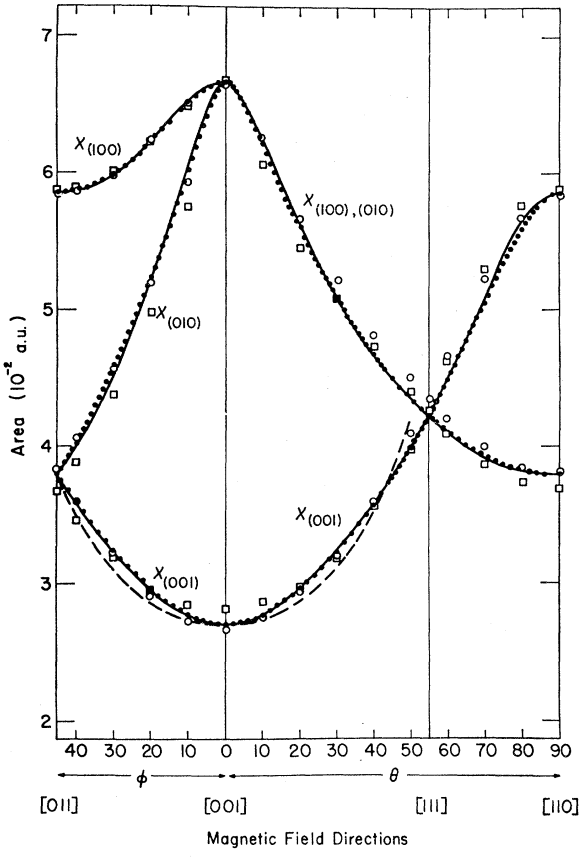

FIG. 2. Extremal area of X pocket as a function of magnetic field direction. Solid dots are Tsui's data (Ref. 14). Solid curve was obtained from his geometrical model. Dashed curve corresponds to extremal areas of a cylinder oriented along the [001] axis. Open squares were obtained in our calculation (Ref. 60) using PS II (zero spin-orbit interaction). Open circles were obtained using PS III which includes spin-orbit and magnetic effects.

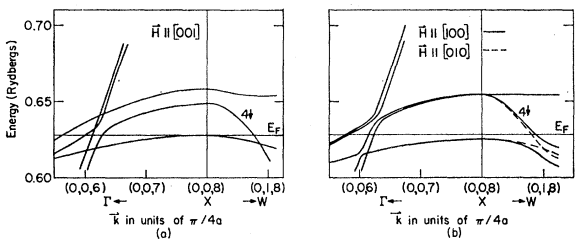

FIG. 3. Comparison of band structures near symmetry point $X=(2\pi/a)(0,0,1)$ (using PS IV) for the magnetic field oriented along the various ⟨001⟩ axes.

from ones calculated from first principles (i.e., APW or KKR methods). Here it is shown that a good fit to the dHvA data can be obtained using our partial two-center approximation, which yields an over-all band structure consistent with the constraints derived from calculated band structures and discussed in Sec. II.

Figure 2 shows the dHvA data of Tsui[14] together with the areas obtained from his geometrical model (solid curve), and the results of two of our semiempirical calculations (open circles and squares).[60] In Fig. 2, $\chi_{(001)}$ represents the extremal area perpendicular to the magnetic field for the pocket along the [001] axis. The open squares represent our results using parameter set II (PS II) without spin-orbit or exchange effects. (See Table III for a list of our parameter sets, which are discussed below.) The open circles represent the case in which these effects are included (PS III).

There are two unusual aspects to the dHvA data: First consider the rapid increase of $\chi_{(001)}$ as the magnetic field is tilted away from the [001] direction. This rise is more rapid than for a cylinder oriented along the [001] direction (dashed line in Fig. 2). Noncentral orbits expected from a dumbbell-shaped surface (as well as from Tsui's geometrical model) have not been observed. This phenomenon has been explained by HSG as arising from combined spin-orbit and magnetization effects.[16,61] These cause the (001) X pocket to increase in volume as the field is tilted away from the [001] direction. We have confirmed this effect, and found the rapid rise to be a function of the *ratio* $\zeta/\Delta E_d$, where ζ and ΔE_d are the spin-orbit and d-band exchange splitting parameters, respectively. Illustrating this effect, Fig. 3 shows the band structure near X at $(2\pi/a)(0,0,1)$ for ⟨001⟩ magnetic field directions. The band structure in the rest of the zone is largely independent of magnetic field direction except where degeneracies are split by spin-orbit interaction, e.g., at L, along Λ, Δ and at accidental degeneracies. In Fig. 3(a) with the field along the pocket major axis, the pocket is considerably smaller than in Fig. 3(b), when the field is normal to this axis.

The second interesting aspect of the data is the anisotropy in $\chi_{(100)}$ as the magnetic field is rotated from the [001] direction to the [011] direction. The extremal area at [001] is 12% larger than the area at

[60] E. I. Zornberg, Solid State Commun. **6**, 729 (1968).

[61] A. V. Gold, J. Appl. Phys. **39**, 768 (1968).

TABLE II. Comparison of pocket dimensions in units of $2\pi/a$ where $a=3.5166$ Å [T. Heumann, Naturwiss **32**, 296 (1944)]. Numbers in italics are dimensions in the central plane normal to the applied magnetic field. These dimensions contribute to the observed dHvA areas. Parameter sets are given in Table III.

Field direction	Location of pockets	HSG[a]			Parameter set III			Parameter set IV		
		$k_{X\Gamma}$	k_{XW}	k_{XU}	$k_{X\Gamma}$	k_{XW}	k_{XU}	$k_{X\Gamma}$	k_{XW}	k_{XU}
[001]	(0, 0, ±1)	0.195	0.100	0.094	0.196	*0.096*	*0.100*	0.213	*0.097*	*0.100*
	(0, ±1, 0)	0.220	0.112	0.108	*0.226*	$k_{X[001]}=0.101$ $k_{X[100]}=0.108$	0.110	*0.231*[b]	$k_{X[001]}=0.101$ $k_{X[100]}=0.110$	0.110
[111]	{(±1, 0, 0) (0, ±1, 0) (0, 0, ±1)}	0.208	0.107	0.098	0.215	0.103	0.110	0.219	0.103	0.110
[110]	(0, 0, ±1)	0.219	0.109	0.103	*0.228*	0.104	$k_{X[\bar{1}10]}=0.106$ $k_{X[110]}=0.113$	*0.230*[b]	0.105	$k_{X[\bar{1}10]}=0.105$ $k_{X[110]}=0.113$
	(0, ±1, 0) (±1, 0, 0)	0.205	0.106	0.102	0.212	0.103	0.106	0.217	0.104	0.105
Dimensions using PS II (no spin-orbit coupling)								0.233	0.098	0.102
Tsui model[c]		0.219	0.105	0.092						

[a] See Ref. 16. [b] Band crossover with $6\uparrow$ accounted for (see Sec. IV, Fig. 7). [c] See Ref. 14.

[011]. This seems to imply that the principal dimension of the pocket k_{XW} (i.e., $k_{X[010]}$) is *greater* than k_{XU} ($k_{X[011]}$). Indeed HSG's calculations and Tsui's geometrical model yield $k_{XW}>k_{XU}$ by 6 and 13%, respectively. On the other hand, it is found that when the two-center constraints are satisfied, k_{XW} is roughly 5% *less* than k_{XU}. In Table II our pocket dimensions are compared (using PS II–IV) with those of HSG[16] and Tsui.[14] Dimensions which contribute to observed dHvA areas are in italics.

Since we obtain an anisotropy in radius of opposite sign to what is expected geometrically, how is our agreement with the area data explained? Two effects are found which contribute to this unexpected agreement. *First*, the agreement is a result of fluting of the Fermi surface such that away from the X face of the BZ, the radius anisotropy gradually changes sign. Figure 4 shows cross sections of the Fermi surface in the (011) (solid curve) and (001) (dashed curve) planes, using PS II. The orbit which has the larger area has the smaller dimension in the X face of the BZ.

This unexpected reversal of the anisotropy is a result of anisotropic interaction with the next lower band, the $X_2\downarrow$ band (i.e., the third minority spin, eighth band over all). Figure 5 shows the band structure (using PS II), normal to [100], in the X face of the zone (solid curves), and in a plane *one-eighth* of the way toward Γ (dashed curves). (For comparison, the major axis of the pocket extends almost *one-quarter* of the way toward Γ.) For clarity, in Fig. 5 the $6\downarrow$ band the flat band from X_5, is left out.

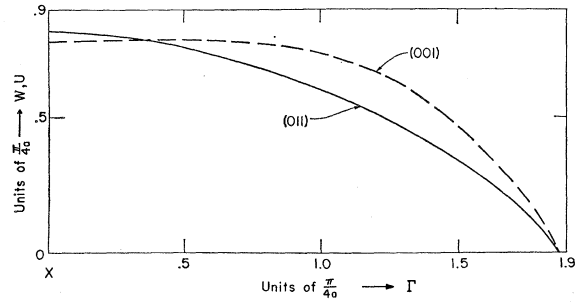

FIG. 4. Extremal cross sections of the pocket at $(2\pi/a)$ (1,0,0) in the (011) (solid curve) and (001) (dashed curve) planes, using PS II.

In the X face of the BZ, the X_2 and X_5 bands have S_4 and S_3 symmetry in the [011] direction and Z_1 and Z_3 symmetry in the [010] direction, respectively.[2,42] Hence in the X face the bands cross along both [011] and [010]. Away from the X face, normal to [100], the bands have − and + symmetry along [011] (compatible with S_4 and S_3)[42] and + and + symmetry along [010] (compatible with Z_1 and Z_3), respectively. As a result the bands from Δ_2 and Δ_5 cross in the [011] direction but are forbidden by symmetry to cross in the [010] direction. The bands in the [010] direction *hybridize* and the upper one bulges out (see Fig. 5). This bulging gives the anisotropy reversal away from the X face, shown in Fig. 4. This effect[60] is the only one available to explain the agreement with the area anisotropy using PS II, in which exchange and spin-orbit parameters are set equal to zero.

When spin-orbit and exchange effects are included, additional band crossings are eliminated. These hybridization splittings can occur near E_F and affect Fermi-surface dimensions. Additional radius anisotropies arise as a consequence of reduced symmetry, resulting from the presence of the magnetic field [see Table II and Fig. 3(b)].

This is the *second* effect which produces the unexpected sign of the area anisotropy. When the field is in the [001] direction, the dimension $k_{X[100]}$ normal to the field is increased. On the other hand, when the field is in the [110] direction, the opposite result is found (see Table II). For the pocket at $(2\pi/a)(0,0,1)$, the bands in the $[\bar{1}10]$ direction, normal to the field, cross while those along the field do not. As a result, $k_{X[100]}$ which contributes to the dHvA area with $\mathbf{H}\|[001]$ [pocket

TABLE III. Parameters of the interpolation scheme (including spin-orbit and exchange interactions), which were obtained fitting *ab initio* calculations and various pieces of experimental information (see Sec. VI).

	Parameter	Units	I	II	III	IV	V	VI	VII
d bands	d_0	Ry	0.532_2	0.532_2	0.532_2	0.585_2	0.62_{52}	0.582_2	0.592_2
	$(dd\sigma)/W$	Ry	-0.038_1	-0.038_1	-0.038_1	-0.038_1	-0.038_1	-0.038_1	-0.038_1
	$(dd\pi)/W$	Ry	0.017	0.017	0.021	0.020	0.020	0.021	0.021
	$(dd\pi')/W$	Ry	0.017	0.017	0.017	0.014	0.014	0.015	0.015
	$(dd\delta)/W$	Ry	−0.0017	−0.0003	−0.0002	−0.0001	−0.0005	−0.0004	−0.0007
d bandwidth	W		1.00[a]	1.00	1.00	1.00	0.90	0.83	0.80
Conduction bands	V_{111}	Ry	−0.006	−0.006	−0.006	−0.015	−0.056	0.009	−0.008
	V_{200}	Ry	0.015	0.015	0.015	0.012	−0.034	0.025	0.012
Orthogonality	A		1.61	1.61	1.61	1.61	1.61	1.61	1.61
	LR_0		2.62	2.62	2.62	2.62	2.62	2.62	2.62
Hybridization	B	Ry	1.48	1.43	1.20	1.40	1.41	1.22	1.17
	LR_1		2.75	2.75	2.75	2.75	2.75	2.75	2.75
Spin-orbit splitting	ζ	Ry	···	0	0.0080	0.0095	0.0084	0.0064	0.0064
Exchange splittings	ΔE_d	Ry	···	0	0.036	0.044	0.040	0.031	0.028
	ΔE_s	Ry	···	0	0	0	0.030	0	0.018
Fermi energy	E_F	Ry	···	0.5569	0.5783	0.6278	0.6581	0.6053	0.6127
	$\zeta/\Delta E_d$				0.22	0.22	0.21	0.21	0.23

[a] By definition.

at (010)] is larger than $k_{X[\bar{1}10]}$ which contributes to the dHvA area with $H\|[110]$ [pocket at (001)].

In Table III the parameters used to fit the X pocket and other data discussed below are shown. Parameter set I (PS I) is our set of starting parameters obtained from fitting our APW results in Sec. II [Ni(Z')]. Parameter set II was used to fit the X pocket without inclusion of spin-orbit or exchange effects. Using these parameters it was not possible to fit the rapid rise in $\chi_{(001)}$ near [001] (see Fig. 2). The bands in Fig. 2(a) of Ref. 60, which were plotted using PS II, are very similar to those plotted here in Fig. 1, using PS I.

The open circles in Fig. 2 were obtained using PS III. In this case it was found useful to apply the partial two-center approximation to get the correct X_5-X_2 separation. The separation of these levels determines the size of the $\chi_{(100)}$ anisotropy.

The partial two-center approximation, which allows separate variation of $(dd\pi)$ and $(dd\pi')$, proves useful for making the Fermi energy ϵ_F obtained from the density of states, agree with the Fermi energy E_F obtained from fitting the X-pocket dHvA data (see Sec. VI). Increasing $(dd\pi)$ raises the upper d-band levels at L and K relative to X_5.[62] This raises ϵ_F [i.e., reduces $n_{tot}(E_F)$, the number of valence electrons/atom], bringing it into better agreement with E_F. Moreover, the level $K_2\downarrow$ is raised above E_F, eliminating an open orbit along Σ which thus far has not been observed.[18,19] At the same time $(dd\pi')$ can be reduced, which lowers X_2 relative to X_5, as required to fit the dHvA data.

Parameter sets IV–VII, which are discussed in detail in Sec. VI, were used to fit the dHvA data, valence [i.e., $n_{tot}(E_F)=10.00$], and various combinations of optical transitions. The fits to the X-pocket dHvA data for these parameter sets are only slightly better than that shown in Fig. 2 for PS III, and therefore they are not shown here. However, a comparison of the fits to *all* the data for *all* of these parameter sets is given in Table V of Sec. VI. The pocket dimensions obtained from these fits are similar to those shown in Table II. The largest differences ($\approx 8\%$) occur in the major axis $k_{X\Gamma}$ when it does not contribute to an observable dHvA area.

While the band structure fits shown in Table I used the two-center approximation, some fits have been made treating the three-center parameters as independent. These are shown in Table IV. Column A is Hodges's fit to Hanus's band structure. Below his parameters, are the two-center parameters which are obtained from various linear combinations[36] of the three-center parameters. These parameters are in good agreement with our d parameters of PS I (column E of Table IV) and our fit to Hanus in Table I. From Table IV it is seen that Hodges's starting parameters obey the two-center approximation quite well. The largest deviation lies in the $(dd\pi)$ values. Similarly, Mueller found

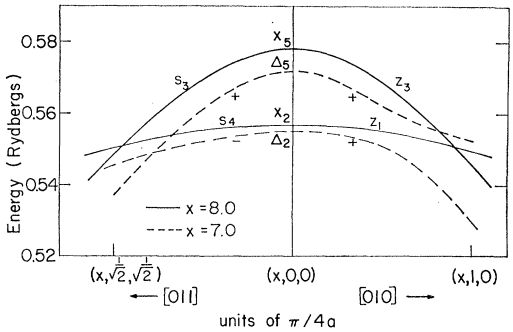

FIG. 5. Bands normal to the [100] axis in the zone face (solid curves), and in a plane one-eighth of the way from X toward Γ (dashed curves), in the [011] and [100] directions, calculated using PS II (zero spin-orbit interaction). For the sake of clarity, the upper X_5 level has been omitted. (The Fermi energy lies at X_2.)

[62] Our L_3 shift was 0.04 eV which is considerably smaller than the 0.2-eV shift proposed in Ref. 27.

TABLE IV. Comparison of d-band parameters in Ry.

Fletcher-Wohlfarth and two-center parameters	Hodges[a] A	B	C	Mueller[b] Cu D	d-band Parameters PS I E	PS IV F
A_1	0.03037	0.03037	0.03654	0.0196		
A_2	0.00899	0.00899	0.01185	0.0061		
A_3	0.01559	0.01559	0.04000	0.0080		
A_4	0.02091	0.02091	0.02091	0.0120		
A_5	0.00413	0.00303	0.00303	0.0026		
A_6	0.01231	0.01340	0.01340	0.0090		
$(dd\sigma)=-(A_1+\frac{2}{3}A_6)$	−0.0386	−0.0393	−0.0454	−0.0256	−0.038	−0.038
$=-\frac{1}{3}(A_4+4A_5)-2A_6$	−0.0371	−0.0378	−0.0378	−0.0256		
$=\frac{1}{2}(-3A_1+\frac{1}{3}(A_4+4A_5))$	−0.0394	−0.0401	−0.0493	−0.0256		
$(dd\pi)=A_2+A_3$	0.0246	0.0246	0.0518	0.0141	0.0173	0.020
$=A_4$	0.0209	0.0209	0.0209	0.012		0.014
$(dd\delta)=-A_1+2A_6$	−0.0058	−0.0036	−0.0097	−0.0016	−0.0017	−0.0001
$=\frac{1}{2}(A_1-A_4-4A_5)$	−0.0035	−0.0016	+0.0035	−0.0016		
$=A_2-A_3$	−0.0066	−0.0066	−0.0282	−0.0019		
$=\frac{1}{3}(2A_6-A_4-4A_5)$	−0.0067	−0.0060	−0.0060	−0.0016		

[a] Used in Refs. 16 and 27. [b] From Ref. 36.

in his fit to Burdick's Cu bands (column D, Table IV) that the main deviation from the two-center approximation is in the $(dd\pi)$ parameters. Therefore, we conclude that one could obtain a considerably better fit to the *ab initio* band structures using the *partial* two-center approximation explained above. However, for our purposes, the differences among the $(dd\sigma)$ and $(dd\delta)$ values in columns A and D in Table IV do not merit going to the full six-parameter FW[47] formalism.

Also shown in Table IV are the d parameters from HEL[27] (column B) and those used by HSG[16] to fit the X pocket (column C). Although the "partial" two-center approximation indicates a *breakdown* of the nearest-neighbor two-center approximation[63] (of order 20% in one parameter), it is considered to be only a "*partial*" *breakdown*. It is not the same as the apparently unrestricted variation of the six FW[47] parameters shown in column C, in which the parameters were allowed to vary by as much as 150%, and constraints 2, 3, 4, and 5 of Sec. II are all violated. In Ref. 60 the band structure obtained using these parameters was compared with that of Hanus, and that obtained from our PS II. *Qualitative* changes were found in the bands at L and X when the two-center approximation is seriously violated in this way.

IV. MAGNETIC BREAKDOWN

In the same experiment discussed in Sec. III, Tsui[14] found an unusual variation in the dHvA amplitude $\chi_{(001)}$, as the applied magnetic field $\mathbf{H}$ was tilted a few degrees (δ) from the [110] direction in the $(1\bar{1}0)$ plane. They found a large signal when $\mathbf{H}$ ($\simeq$30 kG) lies in the symmetry direction ($\delta=0°$), zero signal 1° away, and full signal restored 2° away. TS[14,15] suggested that this effect may be caused by magnetic breakdown[44] (MB) between the neighboring Δ_5 bands ($4\downarrow$ and $5\downarrow$), split by spin-orbit interaction.

Ruvalds and Falicov[52] (RF) showed, using group theoretical arguments, that this effect could be explained as a consequence of breakdown from the $(4\downarrow)$ band to the conduction band of opposite spin ($6\uparrow$). An accidental degeneracy occurs between $\uparrow$ and $\downarrow$ spin bands, when $\mathbf{H}$ lies in the symmetry direction ($\delta=0°$). This degeneracy permits a hole on the pocket Fermi surface to describe a complete orbit *without breakdown*. When $\delta=1°$, a small gap appears between the surfaces. MB can occur across this gap, so that many new orbits are possible. An insufficient number of particles in any particular orbit results in the loss of the dHvA signal. When $\delta>2°$, the gap becomes too large for MB to occur and full signal is restored.

Using our model Hamiltonian we confirmed that the required accidental degeneracy between $\uparrow$ and $\downarrow$ spin bands does occur when the magnetic field lies in the [110] symmetry direction.[64] Our calculations show similar effects for $\chi_{(010)}$ when the magnetic field is near the [001] direction.

In our calculations for this section we found it necessary to include two additional orthogonalized plane waves (OPW's) in our basis set, in order to give a more complete representation of the upper bands near $X=(\pi/4a)(0,8,0)$. Initially our Hamiltonian included four OPW's degenerate at the point $W=(\pi/4a)(4,8,0)$, for the case of zero crystal potential. These are labeled by their principal plane-wave components $(\mathbf{k}+\mathbf{K}_i)$ where the reciprocal-lattice vectors $\mathbf{K}_i$ are[36]

$$\begin{aligned} \mathbf{K}_0&=(0,0,0), & \mathbf{K}_2&=(0,-16,0),\\ \mathbf{K}_1&=(-8,-8,-8), & \mathbf{K}_3&=(-8,-8,8), \end{aligned} \tag{4.1}$$

in units of $\pi/4a$.

[63] Preliminary investigations indicate that the difference between $(dd\pi)$ and $(dd\pi')$ may arise from the neglect of second-neighbor integrals of the type $E_{xy,xy}(100)$ (notation of Ref. 48) which may be large.

[64] E. I. Zornberg, J. Appl. Phys. **40**, 1279 (1969).

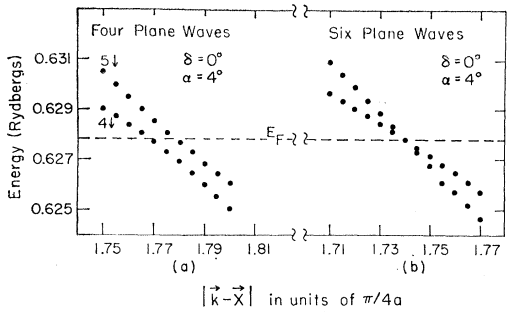

FIG. 6. Band structure near the band crossing at the Fermi energy in the (110) plane (4° off Δ), for applied magnetic field in the [110] direction, using four plane waves and six plane waves in the Mueller interpolation scheme.

The OPW's associated with $\mathbf{K}_0$ and $\mathbf{K}_2$ are degenerate at X in the free-electron approximation. The other two OPW's, $\mathbf{K}_1$ and $\mathbf{K}_3$, are also degenerate at X but at higher energy. Moreover, there are two additional OPW's,

$$\mathbf{K}_4=(8,-8,-8), \quad \mathbf{K}_5=(8,-8,8), \qquad (4.2)$$

in units of $\pi/4a$, which are degenerate with $\mathbf{K}_1$ and $\mathbf{K}_3$ at X. The inclusion of these additional OPW's completes the representation of the upper X_1, X_3, and X_5' levels which have Δ_1, $\Delta_{2'}$, and Δ_5 symmetry, respectively, along Δ.[65] If these states were omitted, then the d band crossing in the (110) plane, required by group theoretic considerations, would be slightly violated. Figure 6 shows in detail bands in the region of the crossing, using four and six plane waves, respectively. When four plane waves are used [Fig. 6(a)] a splitting of 0.0007 Ry occurs for $\delta=0°$. Such a splitting would inhibit orbital crossing and hence the production of a full dHvA signal for this field direction. This small splitting is not caused by first-order hybridization, but arises from higher-order hybridization terms. To treat this effect consistently, the two OPW's (4.2) must be included. When this is done, the crossing required to produce the breakdown effects results. As can be seen from Fig. 6(b), the cancellation of off-diagonal hybridization matrix elements is quite delicate. This suggests that the form factor approach to hybridization is capable of great accuracy ($\simeq$0.0001 Ry in a small region).

On the other hand, the net effect of adding these OPW's, on the band structure away from such crossing points, was small. The largest effect was a downward shift of less than 0.001 Ry in the two lowest Δ_1 bands near X. While in this section our figures were calculated using the six OPW formalism, the four OPW formalism was used in the rest of this work. Eventually the supply of data may make profitable the use of the larger determinant for the entire calculation.[66]

[65] J. C. Slater, *Quantum Theory of Molecules and Solids* (McGraw-Hill Book Co., New York, 1965), Vol. 2.

[66] In fitting the pressure dependence of dHvA areas of Al, P. J. Melz, Phys. Rev. **152**, 540 (1966), found it necessary to use more than four OPW's.

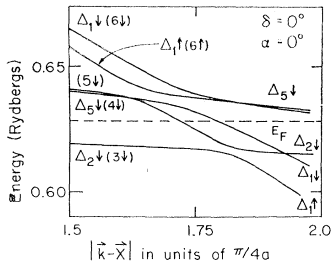

FIG. 7. Band structure in the conduction-band d-band crossover region, in the [001] direction with the magnetic field in the [110] symmetry direction (using the six-plane-wave formalism and PS IV).

Figure 7 shows our band structure (using PS IV) in the MB region along Δ with $\delta=0°$. The s-p conduction bands hybridize with the Δ_5 bands above E_F. As a result the X-pocket Fermi surface has some light-mass conduction-band character along Δ. Band crossings occur along [001] with **H** along [110]. The 5↓ band hybridizes with 6↑ and *crosses* 4↓. The 4↓ band hybridizes with 6↓. MB occurs (for $0°<\delta<2°$) between the (5↓—6↓) band and the (4↓—6↓) bands.

With $\delta=0°$, the band crossing occurs at E_F at an angle of 4° off Δ. For $\delta=1°$, a small splitting of the bands $\simeq$0.001 Ry is obtained.[64] This barrier is sufficiently low that particles can tunnel through.[44] As a result MB occurs, and, as discussed above, the dHvA signal is reduced.

The tunneling probability is given by[44] $P=e^{(-H_0/H)}$, where H_0 is the MB field which is related to the detailed geometry of the orbit.[67] Our calculated results[67] for

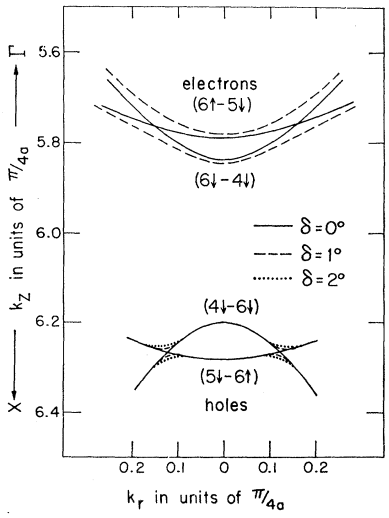

FIG. 8. Details of our Fermi-surface topology (using PS IV with six plane waves) near the ΓX symmetry line, for the applied magnetic field tilted δ° from the [110] direction in the (110) plane. The notation (n-m) refers to a single band which is called n at X and m at the Fermi energy (see Fig. 7). The bands (n-m) and (m-n) have hybridized.

[67] R. G. Chambers, Proc. Phys. Soc. (London) **88**, 701 (1966).

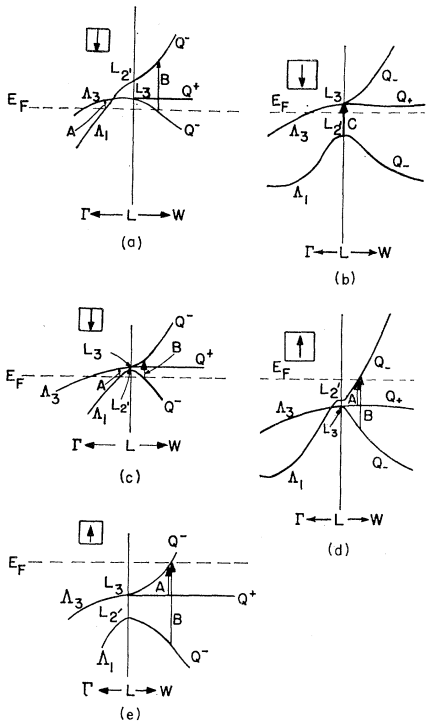

FIG. 9. Five band models showing transitions near L which could give rise to low-energy structure in the interband density of states.

$\delta=1°$, 2°, and 3° gave $H_0=13$, 44, and 115 kG, respectively. As a result, for $\mathbf{H}=30$ kG, $P\approx 50\%$ at $\delta=1.5°$, which is consistent with experiment.

Figure 8 shows our Fermi-surface cross section in the breakdown region. The notation $(n\text{-}m)$ in Fig. 8 refers to a single band in which the position is n at X and m at E_F. The bands $(n\text{-}m)$ and $(m\text{-}n)$ are hybridized. The major differences between Fig. 8 and the results obtained by RF[51] arise from the complex band hybridization shown in Fig. 7. At the bottom of Fig. 8 is shown the X pocket intersecting a large Γ-centered electron surface for $\delta=0°$. The gaps which occur for $\delta=1°$, 2° are indicated.

As shown in Fig. 7, the $6\uparrow$ band, after hybridization with $5\downarrow$, crosses $6\downarrow$ (which has hybridized with $4\downarrow$). This crossover appears in the Fermi-surface cross sections in the upper part of Fig. 8. For $\delta=1°$ this crossover vanishes and a large gap appears. One would therefore expect that when dHvA measurements are made on these large surfaces, MB effects, similar to those found for the X pocket, will appear only for very small $\delta(<0.1°)$.

The above explanation of the MB data places an additional constraint on our band structure. The minority spin d bands must be sufficiently high in energy so that the $\Delta_5\downarrow-\Delta_1\uparrow$ intersection takes place above E_F. This places a lower limit on the position of our $(d\downarrow)$ band relative to the $(s\text{-}p\uparrow)$ conduction band. Band structures IV–VII discussed in Sec. VI all satisfy this constraint, while band structure III does not.

V. OPTICAL SPECTRA

The optical properties of Ni have been measured using a variety of techniques.[23,24,68–73] Structure was first observed in the infrared (near 0.4 eV) using the ferromagnetic Kerr effect.[69] The optical constants of Ni were measured using reflectance by Ehrenreich, Phillip, and Olechna (EPO).[23] They too observed structure in the infrared (near 0.3 eV), as well as weak structure near 1.3 eV. Hanus, Feinleib, and Scouler[24] (HFS) using thermoreflectance, a derivative technique, have found sharp structure at 0.40 eV (0.029 Ry) and at 0.25 eV (0.018 Ry). We refer to this HFS structure as edges α and β, respectively.

We attempt to fit this HFS data, considering direct transitions only and assuming that the structure arises from edges in the interband density of states.[59] We attempt to assign the structure to particular transitions and regions of the BZ. On the basis of these assignments and the other available data, the d band and s-p band exchange splittings are determined.

The HFS data have not been analyzed to yield the imaginary part of the dielectric constant $\epsilon_2(\omega)$. However, structure in the reflectance at a given ω will be qualitatively reproduced in ϵ_2 at almost the same energies.[23]

A number of qualitatively different models have been proposed to explain the infrared edges.[23,24,68,71] Five such models are sketched in Fig. 9. These are all concerned with energy levels near L, since in this region it is possible to have low-energy direct transitions giving rise to edges similar to those observed.

Structure in ϵ_2 may arise either from transitions at critical point energies[74–77] [transition C in Fig. 9(b)] or transitions involving Fermi-surface states[74] [A in Fig. 9(c)]. In general, the latter give rise only to finite discontinuities in the slope of ϵ_2, while the former generate square-root singularities[75,76] with infinite discontinuity in slope (in the absence of lifetime broaden-

[68] For a general review of optical studies of Ni, see H. Ehrenreich, in *Proceedings of the International Colloquim on Optical Properties and Electronic Structure of Metals and Alloys, Paris, 1965*, edited by F. Abeles (North-Holland Publishing Co., Amsterdam, 1966).

[69] G. S. Kirnchik and R. D. Nuralieva, Zh. Eksperim. i Teor. Fiz. **36**, 1022 (1959) [English transl.: Soviet Phys.—JETP **9**, 724 (1959)].

[70] G. S. Krinchik, J. Appl. Phys. **35**, 1089 (1964); G. S. Krinchik and G. M. Nurmukhamedov, Zh. Eksperim. i Teor. Fiz. **48**, 34 (1965) [English transl.: Soviet Phys.—JETP **21**, 22 (1965)].

[71] G. S. Krinchik and E. A. Canshina, Phys. Letters **23**, 294 (1966).

[72] G. S. Krinchik, V. S. Gushchin, and E. A. Canshina, Zh. Eksperim. i Teor. Fiz. Pis'ma v Redaktsiyu **8**, 53 (1968) [English transl.: Soviet Phys.—JETP Letters **8**, 31 (1968)]. They suggest a model similar to our models VI and VII in Sec. VI, omitting a fit to the neck. Their additional structure (A_1 and A_2) occurs at higher energy (>1 eV) in our models.

[73] D. H. Martin, S. Doniach, and K. J. Neal, Phys. Letters **9**, 224 (1964); D. H. Martin, K. J. Neal, and T. J. Dean, Proc. Phys. Soc. (London) **86**, 605 (1965).

[74] J. C. Phillips, Phys. Rev. **133**, A1020 (1964).

[75] L. Van Hove, Phys. Rev. **89**, 1189 (1953).

[76] J. C. Phillips, Phys. Rev. **104**, 1263 (1956).

[77] U. Gerhardt, Phys. Rev. **172**, 651 (1968).

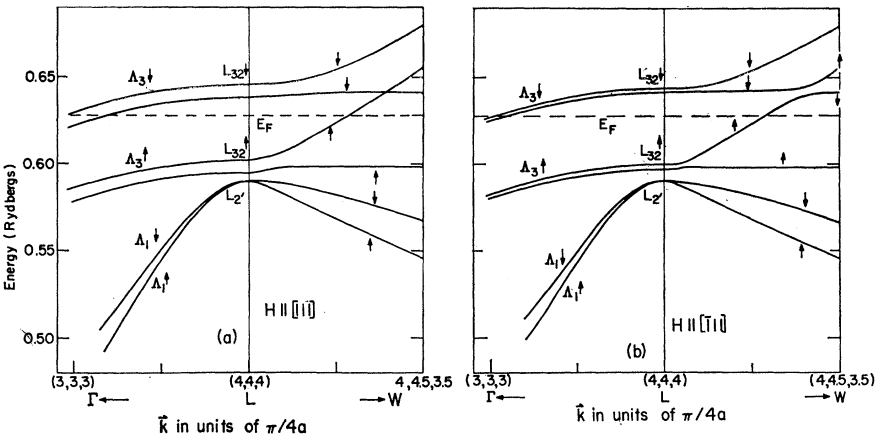

FIG. 10. Band structure near symmetry point $L=(\pi/a)$ (1,1,1) with the magnetic field along (a) the [111] and (b) the [1̄11] directions, using PS IV.

ing). However, when a *line* of Fermi-surface states contributes to the spectrum threshold, again a square-root edge is generated. This is the case for transitions to or from Fermi-surface necks at L, in which there is cylindrical symmetry around ΓL. It is the case for Cu[77] and it presumably also holds for Ni, where the neck radius is one quarter as large.[14]

Models (d) and (e) in the majority spin bands show transitions from Q bands below E_F, to the Fermi-surface neck. One would like to decide between the two models, if possible. Model (d) has $L_{2'}\uparrow$ above $L_{32}\uparrow$, while in model (e) the order of the levels is reversed. In the latter case, the Q^- bands hybridize and the neck band goes into $L_{32}\uparrow$. Both transitions A and B in models (d) and (e) lead to square-root edges in the interband density of states ρ_{mn}. Quadratic expansion of the energy surfaces near L gives ρ_{mn} for edge A six times as large as ρ_{mn} for edge B.

In order to fit the neck radius and shape, it is required that (see Sec. VI, Table VIII)

$$E_F-L_{2'}\uparrow\simeq 0.5\text{ eV}. \tag{5.1}$$

Therefore, whether one has model (d) or (e) now depends on the position of $L_{32}\uparrow$ relative to E_F. The energy difference $E_F-L_{32}\uparrow$ depends in turn on whether one assigns edge α or edge β to transition A. In either case,

$$\hbar\omega_A=E_F-L_{32}\uparrow\leq 0.40\text{ eV}. \tag{5.2}$$

From (5.1) and (5.2) we see that

$$L_{32}\uparrow\geq L_{2'}\uparrow+0.1\text{ eV} \tag{5.3}$$

and therefore only model (e) is satisfactory if one wishes to fit the neck shape and assign either edge α or β to transition A.

The assignment of transition A [of model (e)] determines the position of the *majority* spin d bands relative to E_F, while the X pocket dHvA data and the total density of states determine the position of the *minority* spin d bands with respect to E_F. (Phillips[34] has shown that the X_5, L_{32} separation, relative to the bandwidth, is very nearly independent of the potential used in the calculation.) Assuming rigid bands, one can combine this information to estimate the d-band exchange splitting as follows:

$$\Delta E_d=L_{32}\downarrow-L_{32}\uparrow=(L_{32}\downarrow-E_F)+\hbar\omega_A. \tag{5.4}$$

In Sec. VI (Table VIII) we find

$$L_{32}\downarrow-E_F=0.17\pm 0.04\text{ eV} \tag{5.5}$$

for our band structures which give very nearly 10.00 electrons/atom (PS IV–PS VI). Hence we obtain

$$\Delta E_d=0.57\pm 0.04\text{ eV}\quad(\text{for }\hbar\omega_A=\hbar\omega_\alpha), \tag{5.6}$$

$$=0.42\pm 0.04\text{ eV}\quad(\text{for }\hbar\omega_A=\hbar\omega_\beta). \tag{5.7}$$

Section VI considers band structures for both cases.

Now consider the three models for the minority spin bands near L. Model (b) is the most likely candidate for the minority spin bands for the following reasons:

(1) Transition C of model (b) has a large oscillator strength and gives a critical point square-root edge which is stronger than edges A in models (a) and (c).

(2) Models (a) and (c) require extremely large values of ΔE_s ($>\Delta E_d$) in order that $L_{2'}\downarrow$ lie above E_F, while $L_{2'}\uparrow$ is placed 0.5 eV below E_F to give the correct neck shape [see constraint (6), Sec. II].

(3) Models (a) and (c) predict a hole pocket at L while model (b) does not. This pocket has not been observed in dHvA experiments and TS[14,15] argue that it probably does not exist.

Concluding that model (b) is correct for spin $\downarrow$, one tries to assign to edge C whichever of α or β is left after making the edge A assignment [of model (e)]. Even with model (b) one finds that a relatively large ΔE_s is required to raise $L_{2'}$ so that C is at the required energy:

$$\hbar\omega_C=L_{32}\downarrow-L_{2'}\downarrow=(L_{32}\downarrow-E_F)+(E_F-L_{2'}\uparrow)-(L_{2'}\downarrow-L_{2'}\uparrow), \tag{5.8}$$

$$\simeq 0.17\text{ eV}+0.5\text{ eV}-\Delta E_s \tag{5.9}$$

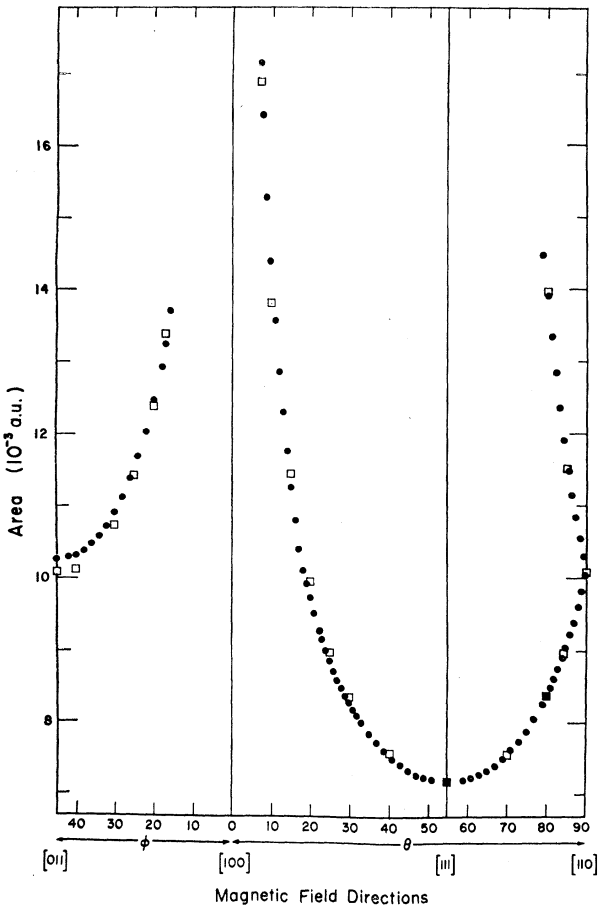

FIG. 11. Angular variation of the dHvA "neck" area in the (100) and (110) symmetry planes. The solid dots are Tsui's data (Ref. 14) and the open squares were obtained using our PS IV.

from (5.5) and (5.1). From (5.9) one obtains

$$\Delta E_s \simeq 0.42 \text{ eV (if } \hbar\omega_C = \hbar\omega_\beta), \tag{5.10}$$

$$\simeq 0.27 \text{ eV (if } \hbar\omega_C = \hbar\omega_\alpha). \tag{5.11}$$

Comparing (5.10) with (5.6), and (5.11) with (5.7), we see that in each case $\Delta E_s > \frac{1}{2}\Delta E_d$. This value of ΔE_s is considered to be rather large, perhaps too large considering the calculations of Connolly[8] and Wakoh[6] (see Sec. II). Therefore calculations for cases in which $\Delta E_s \equiv 0$ are also included. For those cases, $\hbar\omega_C > \hbar\omega_{\alpha,\beta}$. This allows for the possibility that the thermoreflectance data, taken on polycrystalline films, may contain features not intrinsic to pure Ni single crystals.

It should be noted that edge C should give rise to complex structure (at or least wider structure) since the $L_{32}\downarrow$ band is split by spin-orbit interaction. This splitting is a maximum when the magnetic field is parallel to the Λ axis passing through L, and zero when the field is *normal* to this axis.

Figure 10 shows the band structure near $L=(\pi/4a)$ (4,4,4) when the magnetic field is in the [111] and [$\bar{1}$11] directions. From this figure one sees that several transition energies are possible for each magnetic field orientation, corresponding to the various L points which, in the presence of the field, are no longer equivalent. The width of the structure should be a minimum when the field lies in the [100] direction and all the L points are equivalent. When the field is in the [111] direction the width of the structure should be a maximum. It may be possible to detect this variation with field direction ($\approx$0.002 Ry) of the width of the optical structure, and thereby confirm one of the optical assignments, and also determine the spin-orbit and exchange splittings (see Sec. VIII).

VI. COMPLETE FERROMAGNETIC BAND STRUCTURE

So far we have made detailed analyses of the band structure near X and near L. In this section the *complete band structure* is presented and compared with experiment.

The energy bands near X and near L are not unrelated. For example, the transverse mass of the L_{32} state (Q^- neck band) is related, in our model, to the transverse mass of the X_5 state (Z_3) through isotropic hybridization and orthogonality form factors. Therefore we had to fit *simultaneously* the X-pocket data, and the L neck Fermi-surface and optical data. These isotropic form factors also affect both the Δ_1 and Σ_1 bands near E_F, which determine the dimensions of the large sixth band ($\uparrow$ and $\downarrow$ spin) electron surfaces. These dimensions affect the total number of valence electrons $n_{\text{tot}}(E_F)$ which we have attempted to make equal to 10.00/atom.

As mentioned above, dHvA measurements[14,17] have been made on a hyperboloidal neck Fermi surface, similar to what was found in Cu. This Fermi surrace has been ascribed to the sixth majority spin band.[14,27] While in Cu the neck band goes into $L_{2'}$,[2,3] our calculations for Ni in Sec. V showed that it goes into $L_{32}\uparrow$, in agreement with several workers.[8,24,71] As a result, the neck occurs in the tenth band (overall) which is largely a minority spin band (see Fig. 12 below).

Tsui's neck data in two symmetry planes are shown in Fig. 11 (solid dots) together with our extremal areas obtained using PS IV (open squares). There are two main features of these data: the neck radius and the neck shape. The neck radius is obtained from A[111], the extremal area when the magnetic field is in the [111] direction.

From a hyperboloidal expansion of the energy surface near L,[17] one obtains the angular variation of the extremal cross-sectional areas[14,17]:

$$A(\psi) = A[111]/\{\cos\psi[1-(m_t/m_l)\tan^2\psi]^{1/2}\}, \tag{6.1}$$

where the angle ψ is measured from the [111] axis, and m_l and m_t are the longitidinal and transverse masses relative to the [111] axis. Tsui adjusted m_t/m_l to fit

TABLE V. Comparison of our results with experimental data for the parameter sets given in Table III.

		Units	PS III	PS IV	PS V	PS VI	PS VII	Experiment[a]
Optical transition associated with model (e)[b]	edge A		α	α	α	β	β	
with model (b)	edge C		...	...	β	...	α	
Edge energy [using average energy of S.O. split $L_{32}\downarrow$ levels in model (b)]	α	Ry	0.028	0.030	0.028	...	0.029	0.029 (0.40 eV)
	β	Ry	...	...	0.021	0.020	0.019	0.018 (0.25 eV)
Neck: Area	$A[111]$	10^{-2} a.u.	...	0.716	0.716	0.716	0.716	0.716
	$A[110]$	10^{-2} a.u.	...	1.01±0.01	1.02	0.99	1.01	1.02
Shape $\frac{A[110]}{A[111]}$	S		...	1.41	1.43	1.38	1.41	1.43
$X_5\downarrow$ d band hole	[110]	10^{-2} a.u.	2.67	2.70±0.02	2.70	2.70	2.71	2.70
Pocket dHvA areas		10^{-2} a.u.	6.63	6.65±0.03	6.63	6.64	6.68	6.65
For symmetry	[111]	10^{-2} a.u.	4.35	4.29±0.03	4.28	4.28	4.29	4.22
Direction indicated	[110]	10^{-2} a.u.	3.83	3.82±0.03	3.77	3.80	3.81	3.79
		10^{-2} a.u.	5.85	5.87±0.03	5.85	5.85	5.89	5.85
Fast rise of $\chi(001)$ off [001] (see Fig. 2)	$\phi=20°$	10^{-2} a.u.	2.91	2.95±0.02	2.93	2.92	2.94	2.96
Total number of valence electrons/atom	$n_{\text{tot}}(E_F)$	electrons/atom	10.15	10.00±0.02	10.02	10.02	10.08	10.00

[a] Optical data from Ref. 24 and dHvA data from Ref. 14. [b] See Sec. V, Fig. 9.

his data using (6.1) for $\psi<20°$. The ratio m_t/m_l could be used as a measure of the shape of the neck. (This ratio is insensitive to many-body mass enhancement[78–87] because both masses are almost equally affected.[30,81–83]) Instead, for comparison with experiment we use the neck-shape parameter $S=A[110]/A[111]$, which describes the neck over a wider range of angle ψ.

In Table V our values of S and $A[111]$ using PS IV–PS VII are compared with those obtained experimentally. The position of $L_{2'}\uparrow$ was adjusted [by adjusting V_{111}, subject to constraint (1), Sec. II] so that the area $A[111]$ agreed with experiment, i.e., the Fermi energy required to fit the neck radius was made to agree with that obtained from fitting the X pocket.

The neck shape is sensitive to the position of $L_{2'}\uparrow$ relative to E_F, and to the hybridization parameter B, which was determined from fitting the X-pocket data. Fitting the neck shape involves complicated adjustments of the parameters. Since V_{111} and B were adjusted to fit data other than the neck shape, other parameters, such as the d bandwidth W, must be used to influence indirectly the values of V_{111} and B.[88]

The ratio of the major to minor axes of the ellipsoid is well determined by the ratio r_χ defined by

$$r_\chi=\frac{\chi_{(100)} \text{ at } [011]}{\chi_{(001)} \text{ at } [001]}=\frac{0.0585}{0.0270}=2.16. \tag{6.2}$$

The numerator in (6.2) is an extremal area which includes k_{XU} and $k_{X\Gamma}$ (minor and major axes), while the denominator area includes k_{XU} and k_{XW} (both minor axes). Therefore, to good approximation, one can say

$$r_\chi\simeq\frac{k_{XU}k_{X\Gamma}}{k_{XU}k_{XW}}\simeq\frac{k_{X\Gamma}}{k_{XW}}\simeq 2.2, \tag{6.3}$$

using our PS IV dimensions in Table II. This is in good agreement with the experimental results given in (6.2). The hybridization terms affect mainly the minor axes of the ellipsoid. Therefore, r_χ [of (6.2)] was brought into agreement with experiment by adjusting the hybridization parameter B.

Table V compares our values of $n_{\text{tot}}(E_F)$ for PS III–PS VII. The number 10.15, obtained with PS III, is our starting value before adjustment of d_0. While good values of $n_{\text{tot}}(E_F)$ were obtained for PS IV–PS VI, the value of $n_{\text{tot}}(E_F)$ for PS VII is slightly too large. This could have been corrected by increasing d_0 (and reducing W to maintain agreement with S) still further. It would, however, break a pattern among APW and KKR calculations noticed by Connolly,[8] namely, that d bands generally get wider as they are raised with respect to the conduction bands.[89] This agrees with Heine's resonance theory[37] and is further confirmed by calculation on Pd[49] and Pt.[50,90] It is reasonable, con-

[78] J. J. Quinn, in *The Fermi Surface*, edited by W. A. Harrison and M. B. Webb (Wiley-Interscience, Inc., New York, 1960), p. 58.
[79] Reference 22, pp. 290–297.
[80] S. Nakajima and M. Watabe, Progr. Theoret. Phys. (Kyoto) **30**, 772 (1963).
[81] J. C. Phillips and L. F. Mattheiss, Phys. Rev. Letters **11**, 556 (1963).
[82] J. B. Ketterson and L. R. Windmiller, Phys. Rev. Letters **20**, 321 (1968).
[83] L. R. Windmiller, J. B. Ketterson, and S. Hornfeldt, J. Appl. Phys. **40**, 1291 (1969).
[84] K. H. Bennemann, Phys. Letters **25A**, 233 (1967).
[85] K. H. Bennemann, Phys. Rev. **167**, 564 (1968).
[86] N. P. Berk and J. R. Schreiffer, Phys. Rev. Letters **17**, 433 (1966).
[87] S. Doniach and S. Engelsberg, Phys. Rev. Letters **17**, 750 (1966).
[88] Discussion of the details of our parameter variation is available from the author in reprint form.
[89] R. A. Deegan, Phys. Rev. **171**, 659 (1968).
[90] A. R. Mackintosh, Bull. Am. Phys. Soc. **11**, 215 (1966); O. K. Anderson and A. R. Mackintosh, Solid State Commun. **6**, 285 (1968).

TABLE VI. Comparison of results for our ferromagnetic Ni band structures. Parameters are given in Table III.

		Units	PS III	PS IV	PS V	PS VI	PS VII	Experiment
Number of majority spin electrons	$n(\uparrow)$	electrons/atom	···	5.298±0.01	5.307	5.295	5.308[l a]	5.282[b]
Number of minority spin electrons	$n(\downarrow)$	electrons/atom	···	4.700±0.01	4.717	4.730	4.777[l a]	4.718
Number of 6↑ electrons,[b] $[n(\uparrow)-5]$	$n(6\uparrow)$	electrons/atom	···	0.298±0.01	0.307	0.295	0.308[l a]	0.282±0.003
Magneton number $[n(\uparrow)-n(\downarrow)]$	n_-	electrons/atom	···	0.598±0.02	0.590	0.565	0.531[s a]	0.564±0.006[c]
Magneton number $[2n(\uparrow)-10]$	n_-	electrons/atom	···	0.596±0.02	0.614	0.590	0.616[l a]	0.564
Fermi energy derived from density of states	ϵ_F	Ry	0.573	0.6278	$\gtrsim$0.657	0.6049	0.6104	
Fermi energy derived from X pocket (from Table III)	E_F	Ry	0.5783	0.6278	0.6581	0.6053	0.6127[l a]	
d-band exchange splitting from Table III	ΔE_d	eV	0.49	0.60	0.54	0.42	0.38	
s-p band exchange splitting from Table III	ΔE_s	eV	0	0	0.41	0	0.24	

[a] l and s mean that the indicated quantity is too large or too small, because E_F is too large in model VII.
[b] Lowest five ↑ spin bands are filled.
[c] See Eq. (6.5).

sidering that the core states below the conduction bands are very narrow indeed. In the spirit of our calculation, we attempt to conform as much as possible to the results of first principles calculations. Therefore, since the d bands of PS VII are already quite high and narrow, the above adjustments in PS VII were not made at this time. As a result E_F for this case is too large by 0.002 Ry.

Also shown in Table V are our fits to the X-pocket dHvA data. These are quite similar to that shown in Fig. 2 (open circles). There is, however, some improvement over the results of PS III. This improvement is a consequence of the addition of the light-mass s-p band along Δ (see Fig. 7).

Summarizing our parameter variation,[88] it has been found that fitting the X pocket involved fitting: (1) the pocket size using E_F, (2) the ratio r_χ (6.2) using the hybridization B, (3) the $\chi_{(100)}$ anisotropy using $(dd\pi')$, $(dd\delta)$, and (4) the rapid rise of $\chi_{(001)}$ using spin-orbit parameter ζ.

Fitting the neck involved fitting (1) the size $A[111]$ using V_{111}, and (2) the shape S using indirectly the bandwidth W. The fit to $n_{tot}(E_F)$ was made by adjusting d_0 and $(dd\pi)$. MB data also implied an increase in d_0. The optical data were fitted by adjusting the exchange splittings ΔE_d and ΔE_s.

The analysis of the optical experiments was inconclusive. Therefore, band structures for four cases are presented: PS IV was adjusted so that the transition A [model (e)] in the majority spin bands agreed with edge α (0.40 eV). PS VI was similarly adjusted to fit edge β (0.25 eV). The s-p exchange splitting ΔE_s was set equal to zero for these cases, in agreement with the results of Connolly[8] and considering constraint (6), Sec. II.

If one ignores this constraint one can fit both edges simultaneously, as demonstrated by PS V and PS VII. In PS V edge α is assigned to transition A and edge β to transition C. In PS VII the assignments are reversed. We cannot, at this time, say which of the four optical assignments is most likely to be correct.

Hanus *et al.*[91] argue in favor of model VII over model V. Using the dHvA neck data and experimental effective mass, they obtain

$$E_F - L_{32\downarrow} = (\hbar^2/2\pi)(A[111]/m_l^*[111]) = 0.11 \text{ eV}. \quad (6.4)$$

TABLE VII. Predicted extremal areas and radii of large Γ-centered electron Fermi surfaces, for magnetic field along [001]. Radii are in units of $(\pi/4a)$ where a is the lattice constant (given in Table II).

	Band	PS III	PS IV	PS V	PS VI	PS VII
Area (a.u.)	10	[a]	2.05	2.08	2.09	2.13
	11	1.21	1.18	1.21	1.17	1.21
	12	0.93	0.86	0.86	0.88	0.92
Radius, units of $(\pi/4a)$						
[100] direction	10		6.16	6.09	6.13	6.13
	11		5.81	5.87	5.91	5.99
	12		5.73	5.79	5.86	5.93
[110] direction	10		8.21	8.24	8.30	8.39
	11		4.69	4.75	4.66	4.76
	12		3.80	3.82	3.87	3.97

[a] Open orbit.

[91] J. Hanus, J. Feinleib, and W. J. Scouler, J. Appl. Phys. **39**, 1272 (1968).

TABLE VIII. Energy differences between the Fermi energy and levels at the symmetry points X, L, W for our intermediate (PS III) and final band structures (PS IV–PS III). The symbol $\langle\ \rangle$ means the average energy of a set of spin-orbit split levels, and $[E(X_2\downarrow)]_{\max}$ and $[E(X_2\downarrow)]_{\min}$ are the maximum and minimum energies of the $X_2\downarrow$ level.

Energy difference (Ry)		PS III	PS IV	PS V	PS VI	PS VII
$E_F-E(L_2'\uparrow)$	ϵ_1	−0.003[a]	0.038	0.040	0.040	0.039
$\langle E(L_{32}\downarrow)\rangle-E_F$	ϵ_2	0.008	0.0145	0.0115	0.011	0.008[s b]
$\langle E(L_{32}\downarrow)\rangle-E(L_2'\downarrow)=\hbar\omega_C$	ϵ_3	0.005[a]	0.052	0.021	0.051	0.029
$E_F-\langle E(L_{32}\uparrow)\rangle=E_f$(neck)$=\hbar\omega_A$	ϵ_4	0.028	0.030	0.028	0.020	0.019
$\langle E(X_5\downarrow)\rangle-E_F=E_f$ (pocket)	ϵ_5	0.018	0.0257	0.0222	0.0194	0.117[s b]
$E_F-[E(X_2\downarrow)]_{\max}$	ϵ_6	0.0012	0.000	−0.0001	−0.0004	−0.0002
$E_F-[E(X_2\downarrow)]_{\min}$	ϵ_7	0.0036	0.003	0.002	0.0015	0.002
$E(K_2\downarrow)-E_F$	ϵ_8	−0.0026	0.0043	0.0034	0.0023	0.0011
$E(W_1'\downarrow)-E(W_1\downarrow)$	ϵ_9	0.087	0.094	0.095	0.075	0.072

[a] L_2' was not adjusted using V_{111} to give the neck radius; as a result PS III gives no neck.
[b] s means quantity is too small because E_F is too large in model VII.

Allowing for mass enhancement they argue that the 0.11-eV energy is too small to give 0.40 eV for edge A. On the other hand, 0.40 eV was obtained for edge A in models IV and V, and moreover our mass enhancement is only ≈ 2 (see Sec. VII). Their error occurs in using the effective mass at the Fermi energy (0.25) as a good approximation to the over-all effective mass of the Q_- neck band near L.

For each of our band structures we calculated the magneton number $n_-=n(\uparrow)-n(\downarrow)$. If $n_{\rm tot}(E_F)\equiv n(\downarrow)+n(\uparrow)=10.00$, then $n_-=2n(\uparrow)-10.00$. Table VI compares values of n_- from both expressions. The differences are a consequence of $n_{\rm tot}(E_F)\neq 10.00$.

We can estimate n_- experimentally from knowledge of the saturation magnetization M_s and the average of factor $\langle g\rangle$[74,81]:

$$n_-=n(\uparrow)-n(\downarrow)=(2/\langle g\rangle)M_s$$
$$=0.564\pm0.006 \text{ electrons/atom}, \quad (6.5)$$

where $M_s=0.6155\pm0.006$ bohr magnetons,[25] and $\langle g\rangle=2.18\pm0.02$.[26,92–94] Our calculated values of n_- in Table IV are $\approx 6\%$ larger than the result of (6.5). This discrepancy may imply that $\langle g\rangle$ used in (6.5) was too large. (For Pd g has been found to be highly anisotropic.[83]) Our value of $n_-(\approx 0.60)$ implies that $\langle g\rangle=2.05$.

Table VI also compares E_F (obtained from fitting the X pocket) with ϵ_F (obtained from the density of states). These should be compared with the deviation of $n_{\rm tot}(E_F)$ from 10.00 electrons/atom shown in Table V. The differences between E_F and ϵ_F are very small because of the large density of states at the Fermi energy (≈ 2 electrons/atom eV).

Also included in Table VI are our exchange splittings (from Table III) in eV. The d band splittings all fall in the range 0.4–0.6 eV. This is about half the values estimated by Connolly[8] and Wakoh[6] using "optimum" one-electron potentials. This discrepancy confirms the importance of the semiempirical approach adopted here.

Table VII gives our predictions of belly areas and radii for the large Fermi surfaces for our various band structures. Orbital crossings, such as that shown at the top of Fig. 8, were ignored in these calculations.

Table VIII shows energy differences between E_F and levels at X and L. The $X_2\downarrow$ level shifts with changing magnetic field direction. Its energy at $X=(2\pi/a)(0,0,1)$ decreases by $\simeq 0.003$ Ry when the magnetic field is tilted from the [001] to the [010] direction (for PS IV). Therefore, from ϵ_6 and ϵ_7 in Table VIII (PS V–PS VII), it is concluded that there *may* be a small heavy mass X_2 pocket for some field directions. However, from the results of PS IV and the small values of ϵ_6, there need not be such a pocket. It has not been observed experimentally.

We found that fitting the neck shape and radius required $\epsilon_1\simeq 0.040$ Ry. This result was used in Sec. V, together with ϵ_2 to estimate the exchange splittings required to fit the optical transitions. The ϵ_3 and ϵ_4 energies correspond to transitions C and A. The energy ϵ_3 is included also for those cases in which an attempt was not made to fit both transitions (i.e., with $\Delta E_s=0$). The ϵ_5 energies show the range of X-pocket Fermi widths which are possible. Raising the d bands results in lower E_F (relative to X_5) and therefore larger ϵ_5. The energy ϵ_8 indicates whether the large tenth-band electron surface is open (negative ϵ_8) or closed (positive ϵ_8). The energy ϵ_8 is small (≈ 0.003 Ry) and decreases with decreasing $(dd\pi)$. Therefore the topology of this surface is in doubt. However, from consideration of $n_{\rm tot}(E_F)$ it seems more likely that ϵ_8 is positive and the surface is closed.

Hanus *et al.*[91] suggested assigning the weak 1.3-eV structure to the $W_1'\downarrow-W_1\downarrow$ transition. From the values of ϵ_9 in Table VIII, it is seen that our band structures IV and V agree with this assignment while VI and VIII, having narrower d bands, do not.

[92] D. S. Rodbell [in *Proceedings of the International Conference on Magnetism, Nottingham, 1964* (The Institute of Physics and the Physical Society, London, 1965)] obtained $g=2.22$.
[93] H. W. DeWijn and J. J. M. Franse [Phys. Letters **21**, 9 (1966)] obtained $g=2.27$.
[94] The workers in Ref. 26 believed that others (Refs. 92 and 93) obtained higher g values because of adsorbed gases; A. J. P. Meyer (private communication).

TABLE IX. Energy levels at symmetry points with the magnetic field along [001] (Ry).

	PS IV					PS V				
Band	(000)	$X(080)$	$X(008)$	$L(444)$	$W(480)$	(000)	$X(080)$	$X(008)$	$L(444)$	$W(480)$
12	0.5670	0.7968	0.7968	0.6446	1.0802	0.6006	0.8617	0.8617	0.6717	0.9653
11	0.5665	0.7968	0.7968	0.6404	1.0788	0.6002	0.6317	0.8317	0.6679	0.9346
10	0.5263	0.6546	0.6584	0.6004	0.6534	0.5635	0.6813	0.6847	0.6484	0.6803
9	0.5248	0.6541	0.6485	0.5961	0.6095	0.5622	0.6808	0.6759	0.6315	0.6404
8	0.5076	0.6249	0.6278	0.5900	0.5589	0.5469	0.6558	0.6582	0.6276	0.5855
7	0.5038	0.6093	0.6109	0.5899	0.5167	0.5435	0.6402	0.6419	0.6184	0.5465
6	0.4941	0.6077	0.6046	0.4813	0.4266	0.5349	0.6389	0.6360	0.5259	0.4698
5	0.4628	0.5799	0.5803	0.4718	0.4263	0.5062	0.6150	0.6153	0.5175	0.4695
4	0.4572	0.3299	0.3300	0.4351	0.3862	0.5013	0.3883	0.3883	0.4840	0.4306
3	0.4538	0.3001	0.3000	0.4257	0.3849	0.4983	0.3485	0.3484	0.4757	0.4296
2	−0.0688	0.2864	0.2864	0.2794	0.3743	−0.0563	0.3337	0.3337	0.3004	0.4175
1	−0.0689	0.2616	0.2616	0.2452	0.3356	−0.0864	0.2953	0.2953	0.2632	0.3795
	PS VI					PS VII				
Band	(000)	$X(080)$	$X(008)$	$L(444)$	$W(480)$	(000)	$X(080)$	$X(008)$	$L(444)$	$W(480)$
12	0.5560	0.7827	0.7827	0.6174	1.1367	0.5625	0.8058	0.8058	0.6226	1.0935
11	0.5558	0.7827	0.7827	0.6146	1.1360	0.5623	0.7878	0.7878	0.6199	1.0753
10	0.5263	0.6253	0.6280	0.5863	0.6246	0.5357	0.6307	0.6333	0.5944	0.6299
9	0.5256	0.6250	0.6213	0.5834	0.5936	0.5350	0.6304	0.6266	0.5921	0.6019
8	0.5053	0.6037	0.6057	0.5649	0.5498	0.5136	0.6106	0.6129	0.5916	0.5578
7	0.5023	0.5935	0.5945	0.5649	0.5196	0.5106	0.6018	0.6025	0.5741	0.5302
6	0.4966	0.5924	0.5903	0.4821	0.4369	0.5050	0.6006	0.5986	0.4932	0.4520
5	0.4732	0.5720	0.5722	0.4757	0.4368	0.4844	0.5819	0.5821	0.4869	0.4518
4	0.4696	0.3542	0.3542	0.4497	0.4077	0.4808	0.3702	0.3703	0.4636	0.4242
3	0.4672	0.3284	0.3283	0.4434	0.4073	0.4785	0.3449	0.3449	0.4574	0.4238
2	−0.0689	0.3235	0.3235	0.3127	0.3909	−0.0597	0.3424	0.3424	0.3259	0.4084
1	−0.0689	0.3008	0.3008	0.2880	0.3627	−0.0777	0.3181	0.3181	0.3001	0.3816

Table IX lists the 12 lowest eigenvalues at symmetry points Γ, X, L, and W, for the magnetic field in the [001] direction.

Figure 12 shows our ferromagnetic band structure using PS IV for **H** parallel to [001]. In both Table IX and Fig. 12, two X points are shown, which are not equivalent in the presence of the magnetic field.

VII. COMPARISON WITH EXPERIMENT

A. Effective Masses

By measuring the temperature dependence of the dHvA amplitude, Tsui[14] obtained cyclotron effective masses m^* of the X-pocket and L-neck Fermi-surface orbits. These masses can be compared with the one-electron-band-structure masses m_b obtained from[3]

$$\frac{m_b}{m_0}=\frac{\hbar^2}{2\pi}\frac{\partial A}{\partial E}\bigg|_{E=E_F} \tag{7.1}$$

where m_0 is the ordinary electron mass and A is the cross-sectional area of a constant energy surface of energy E, normal to the magnetic field. The masses obtained from (7.1) are generally smaller than those found experimentally.[3,30,82–83] The difference has been attributed to many-body effects such as electron-electron, electron-phonon,[78–80] and electron-magnon interactions.[84–85] The mass enhancement factor α is defined by[3]

$$\alpha=m^*/m_b=\text{experimental mass/band-structure mass.} \tag{7.2}$$

TABLE X. Effective masses and mass enhancement.

Fermi surface	Symmetry directions	Experiment[a]		PS II		PS III		PS IV	
		area in 10^{-2} a.u.	mass m^*/m_0	m_b/m_0	m^*/m_b	m_b/m_0	m^*/m_b	m_b/m_0	m^*/m_b
Spin ↑ s-band neck	[111]	0.716	0.25±0.02					0.13±0.01	1.9±0.2
	[110]	1.02	0.36±0.02					0.20±0.01	1.8±0.2
X_5↓ d-band hole pocket	[100]	2.70	1.0 ± 0.1	0.48	2.0	0.50	2.0	0.45±0.03	2.2±0.3
	($\theta=7°$)	6.65 (at $\theta=0°$)	1.9 ± 0.2	1.44	1.3	1.38	1.4	0.89±0.03	2.1±0.3
	[110]	3.79	1.35± 0.1	0.72	1.9	0.75	1.8	0.70±0.03	1.9±0.2
		5.85	1.4 ± 0.3	0.85	1.6	0.85	1.6	0.62±0.03	2.3±0.4
Large belly surfaces band 10	[001]							8 ±1	
11								2.9 ± 0.2	
12	[001]							3.7 ± 0.2	

[a] See Ref. 14.

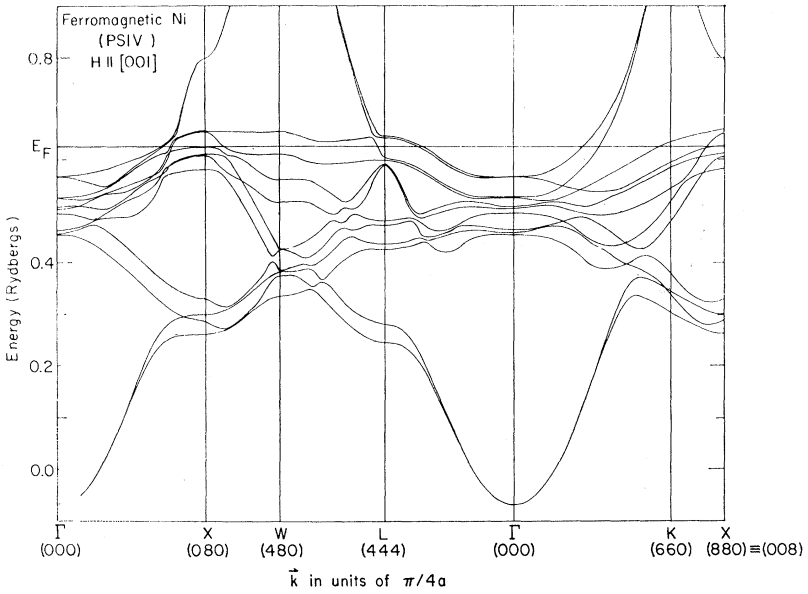

FIG. 12. Ferromagnetic band structure using PS IV with magnetic field along [001].

Table X compares the experimental and calculated effective masses and presents the mass enhancement factor α, for various extremal orbits using PS II–IV. For PS IV it is found that the mass enhancement is *nearly uniform* for both Fermi surfaces. This uniformity is not found using PS II (unshifted d bands and no spin-orbit interaction) or PS III (unshifted d bands). Raising the d bands added light-mass s-p character to orbits which pass near the breakdown region near Δ. As a result, the band effective masses for the larger orbits were reduced, bringing the mass-enahncement factor into agreement with numbers found for the smaller orbits.

This uniformity of mass enhancement for a given Fermi surface agrees with results obtained for Cu,[30] Pd, and Pt.[82,83] Therefore one can say that mass enhancement results provide further evidence of the partial s-p character of the X pocket.

Table X also estimates the effective masses of the large Γ-centered electron surfaces. The mass of the surface in band 10 is very large, which would make the dHvA signal difficult to observe. Nevertheless, *some* large Γ-centered electron surface orbits are now being observed in dHvA experiments.[43]

B. Density of States

Early photoemission experiments[95] on Ni showed an anomalous strong peak in the density of states (DOS) ≈ 5 eV below E_F. This peak could not be explained using accepted one-electron band calculations. Other experiments, using a variety of techniques,[96–98] all show instead a large DOS peak for Ni within 2 eV of the Fermi energy. However, more recent ultraviolet photoemission results[45] also do not contain the large peak 5 eV below E_F. These results are shown in Fig. 13, together with our DOS for PS IV and VI, calculated using the Quad scheme.[99] Energies were obtained at 343 000 points in one-eighth of the zone. While our DOS show more structure than the experimental data, the overall features are similar, with structure occurring at nearly the same energies.

The major peaks in the DOS occur just below the exchange split L_{32} levels. Therefore the experimental data, which contain a large peak at -0.2 eV relative to E_F, favors model VI in which

$$E_F - L_{32}\uparrow = \hbar\omega_A = \hbar\omega_\beta = 0.25 \text{ eV} \qquad (7.3)$$

over model IV in which $\hbar\omega_A = 0.40$ eV. However, the error in the position of the experimental structure may be as large as 0.2 eV.[100]

The main differences between the DOS in Figs. 13(a) and (b) exist because the d bands for PS VI are more narrow and less exchange split than those for PS IV. The ultraviolet photoemission data[45] appear to favor the smaller exchange (PS VI) and the broader d bands (PS IV). The other experiments,[96–98] which showed less structure, gave a dominant peak near 1 eV. They were inconclusive, as far as helping us choose between our models.

Figure 14 shows the paramagnetic DOS using PS IV without spin-orbit or exchange splittings. The sharp structure in Fig. 13(a) can be easily identified with peaks in Fig. 14.

[95] A. J. Blodgett, Jr., and W. E. Spicer, Phys. Rev. **146**, 390 (1966).
[96] J. R. Cuthill, A. J. McAlister, M. L. Williams, and R. E. Watson, Phys. Rev. **164**, 1006 (1967).
[97] H. D. Hagstrum, Phys. Rev. **150**, 495 (1966); H. D. Hagstrum and G. E. Becker, *ibid.* **159**, 572 (1967).
[98] C. S. Fadley and D. A. Shirley, Phys. Rev. Letters **21**, 980 (1968).
[99] F. M. Mueller, J. W. Garland, M. H. Cohen, and K. H. Bennemann (unpublished).
[100] D. E. Eastman (private communication).

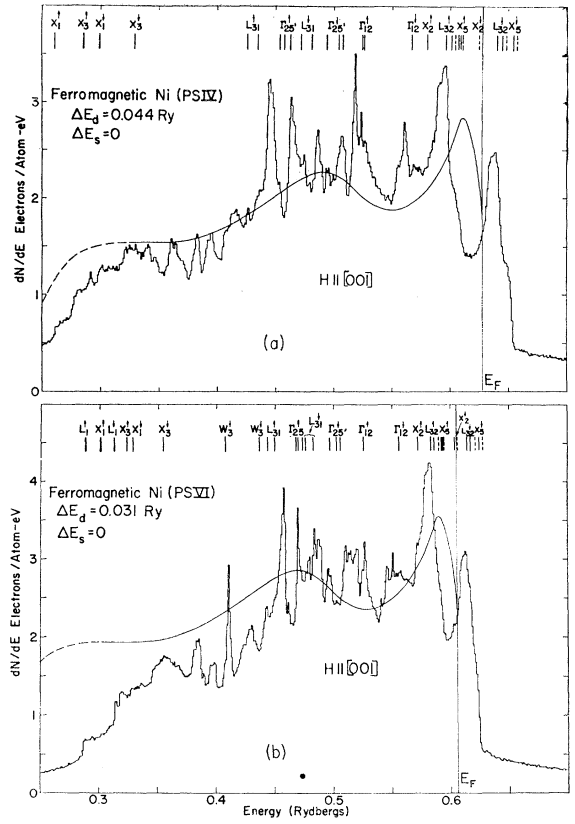

FIG. 13. Densities of states of ferromagnetic Ni using PS IV and VI with magnetic field along [001]. [Note difference in vertical scale between (a) and (b)]. Symmetry point energies are shown by vertical lines above each curve. The dashed lines among these, corrsepond to the X levels on the [001] axis, along the magnetic field (see Table IX). Superimposed on each curve is the photoemission data from Ref. 45 (smooth curve).

VIII. CONCLUSIONS

Band structures of ferromagnetic Ni were constructed which give detailed agreement to experimental data, where available, and over-all agreement to the results of *ab initio* calculations. In particular, we fit the X-pocket and L-neck dHvA data, MB effects, optical edges and valence (i.e., 10.00 electrons/atom). The magneton number, the effective masses, and the DOS were calculated and compared with experiment. Estimates were also made of the dimensions and masses for the large Γ-centered Fermi surfaces, which have not yet been measured in detail.

It was possible to fit the X pocket and other data using a "partial" two-center approximation to the tight-binding d parameters. The $X_5\downarrow$ pocket was found to have unusual shape resulting from anisotropic interaction with the neighboring $X_2\downarrow$ band. It was found that symmetry, and the loss of it because of the presence of the magnetic field, played a major role in determining the X-pocket anisotropy. The position of $X_2\downarrow$ relative to $X_5\downarrow$ was important for fitting the dHvA data. The $X_2\downarrow$ band lies so close to the Fermi energy that it is still not possible to say that an X_2 pocket does not exist, except insofar as it has not been observed. It may exist for some field directions and not for others (see Sec. VI).

It was found that in order to fit the rapid rise of $\chi_{(001)}$, it is necessary that (see Table III)

$$\zeta/\Delta E_d = 0.22 \pm 0.01. \tag{8.1}$$

Therefore if the spin-orbit splitting parameter ζ were known, one could deduce the d-band exchange ΔE_d. If one uses the atomic value of ζ ($\zeta_{\text{at}} \approx 0.07$ eV), one obtains $\Delta E_d = 0.32$ eV. In a crystal $\zeta > \zeta_{\text{at}}$[16,36,101,102] (e.g., for Pb,[101] $\zeta = 1.5\zeta_{\text{at}}$). Therefore our exchange splittings of 0.4–0.6 eV are reasonable.

These values of the exchange splitting are to be compared with thermodynamic estimates[103–107] of 0.2–0.35 eV and "first-principles" estimates[6,8] of 1 eV, based on plausible local potentials. The discrepancy in the former case is explained by the failure in the thermodynamic model to include many-body mass enhancement,[78–87] which would increase their value by a factor of 2 (see Sec. VII A). In the latter case it appears that the true nonlocal exchange gives rise to smaller exchange splittings than one would estimate from any plausible local potential.[29,30]

Our values of the exchange splittings were dependent on the assignments of optical data taken on polycrystalline Ni films.[24] One is dependent on this data because the majority spin d band lies entirely below the Fermi energy, so that its position is difficult to estimate using Fermi-surface data alone. Further optical experiments on single crystals using a variety of (or modulating) magnetic field orientations could make our optical assignments more conclusive (see Sec. V). At the same time, it may be possible to measure ζ and deduce ΔE_d from (8.1).

In fitting the experimental data, it was found necessary to shift the d bands up (≈ 0.05 Ry) relative to what was obtained from our APW calculation. This shift, which added s-p character to the X pocket along its major axis, (1) improved the X-pocket fit, (2) helped explain the MB effects, (3) made the mass enhancement of the X-pocket orbits more uniform, and (4) decreased the Fermi energy (relative to X_5) needed to fit the X pocket so that the total number of valence electrons was 10.00/atom.

[101] J. R. Anderson and A. V. Gold, Phys. Rev. **139**, A1459 (1965).
[102] R. Braunstein and E. O. Kane, J. Phys. Chem. Solids **23**, 1423 (1962).
[103] For estimates of exchange splittings in Ni, using various techniques, see E. P. Wohlfarth, in *Proceedings of the International Conference on Magnetism, Nottingham, 1964* (Institute of Physics and the Physical Society, London, 1965), p. 51; J. C. Phillips, J. Appl. Phys. **39**, 758 (1968).
[104] E. P. Wohlfarth, Phil. Mag. **42**, 374 (1951).
[105] M. Shimizu, T. Takohashi, and A. Katniki, J. Phys. Soc. Japan **18**, 801 (1963).
[106] M. Shimizu, Proc. Phys. Soc. **84**, 397 (1964).
[107] E. D. Thompson, E. P. Wohlfarth, and A. C. Bryan, Proc. Phys. Soc. (London) **83**, 59 (1964).

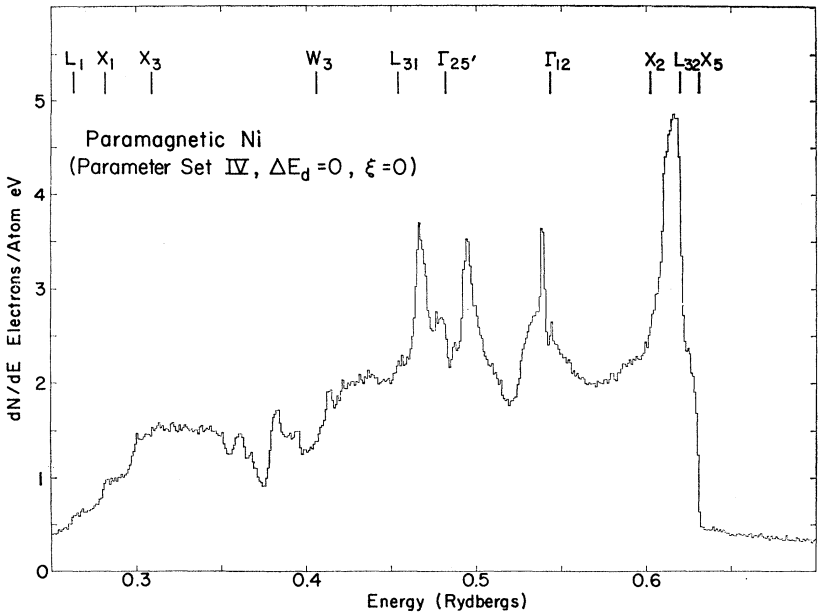

FIG. 14. Density of states of paramagnetic Ni using PS IV without spin-orbit or exchange splitting.

This d-band shift and the exchange splitting caused $L_{32}\downarrow$ to be above $L_{2'}\downarrow$ in agreement with KC[71] and Connolly.[8] Therefore no $L_{2'}\downarrow$ hole pocket is expected. On the basis of our fit to the neck shape and the optical edges, it was decided that $L_{32}\uparrow$ was probably above $L_{2'}\uparrow$.

It was found that the accidental degeneracy necessary to explain the MB data could be obtained, if two OPW's were added to our basis set. The delicate cancellation of off-diagonal matrix elements could then be obtained in the framework of Mueller's interpolation scheme.

Our DOS were in good agreement with the recent ultraviolet photoemission data[45] which do not show the spurious peak at low energy.[95]

Seven sets of parameters have been presented, including PS I which was our starting set. PS II and PS III showed the necessity of including spin-orbit coupling and illustrated our model of the X pocket. PS IV–PS VII fit all the data considered, except that PS VII gave too many electrons/atom. Table V compared with experiment all our results obtained from PS III–PS VII. While at present it is difficult to say which of PS IV–PS VII is most likely to be correct, one tends to favor PS IV and PS VI since PS V and PS VII require $\Delta E_s > \frac{1}{2}\Delta E_d$.

Even though more parameters were available than there were pieces of experimental information, it was possible to constrain our parameters on the basis of earlier APW and KKR calculations. Fitting the data enabled us to reduce further the parameter space available. Additional dHvA experiments on the large Fermi surfaces can confine the region of parameter space under consideration even more, while single-crystal optical experiments may make the band structure very well known indeed.

ACKNOWLEDGMENTS

It is a pleasure to thank Professor J. C. Phillips for suggesting this line of research, and to thank him, Professor M. H. Cohen, and Dr. F. M. Mueller for taking a continuous interest in it, and for offering numerous helpful suggestions. I am particularly indebted to Professor R. W. Stark and Dr. D. C. Tsui for discussions of the experimental data. I have also benefited from conversations with Professor L. M. Falicov and Professor P. Soven, and Dr. U. Gerhardt, Dr. J. Ruvalds, and Dr. R. Sandrock. Support of this research by the National Aeronautics and Space Administration and the Advanced Research Projects Agency is gratefully acknowledged. Portions of this work were done at Argonne National Laboratory which is supported by the U. S. Atomic Energy Commission.